

CHAPTER 14

Structural Diversity in Metal Phosphonate Frameworks: Impact on Applications

KONSTANTINOS D. DEMADIS AND NIKOLETA STAVGIANOUDAKI

Crystal Engineering, Growth & Design Laboratory, Department of Chemistry, University of Crete, Heraklion, Crete, GR-71003, Greece

14.1 Introduction

The emerging fields of supramolecular chemistry, crystal engineering, and materials chemistry have made long strides forward with impressive growth during the last decades. The chemistry of phosphonate ligands has undoubtedly played an important role in widening these areas of research.^{1–42} Phosphonate ligands have attracted considerable attention in the context of fundamental research, but they have also been extensively used in several other technologically/industrially significant areas, such as water treatment,^{43–46} oilfield drilling,^{47–54} minerals processing,^{55,56} corrosion control,^{57–62} metal complexation and sequestration,^{63,64} dental materials,^{65–68} enzyme inhibition,^{69–71} bone targeting,^{72–75} cancer treatment,^{76–78} etc. There exists a plethora of metal phosphonate materials whose crystal structures exhibit attractive features that depend on several variables, such as nature of M^{n+} (metal oxidation state, ionic radius, and coordination number in particular), number of phosphonate groups on the ligand backbone, presence of other functional moieties (carboxylate, sulfonate, amine, hydroxyl), and, naturally, on process variables (reactant ratio and concentration, temperature, pressure, etc.). The synthesis of metal phosphonates is usually carried out in aqueous solutions (or in mixtures of water and a polar organic solvent such as alcohols, DMF, acetone), so it is

Metal Phosphonate Chemistry: From Synthesis to Applications

Edited by Abraham Clearfield and Konstantinos Demadis

© Royal Society of Chemistry 2012

Published by the Royal Society of Chemistry, www.rsc.org

not surprising that water is commonly found in their lattice, participating in extensive hydrogen bonding, which is predominant in these architectures resulting in 1D, 2D, and 3D supramolecular networks.^{79–81} Lastly, it is worth noting that the vast majority of metal phosphonates are coordination polymers and clusters (to a lesser extent), although there are reports of metal phosphonate molecular complexes.

The structural literature of metal phosphonate materials is fairly large. However, in this chapter we will present a selective overview, focusing on some interesting structural features of metal phosphonate materials that contain metal ions in a variety of oxidation states combined with a diverse selection of phosphonate ligands. We will also explore possible relationships between structural features and properties, with an eye towards applications. The structures of the phosphonate ligands (and their “mixed” analogs) mentioned in this chapter are shown in Figure 14.1.

14.2 The P–O Bond in “Free” Phosphonic Acids and “Metal-coordinated” Phosphonates

The phosphonate group is a strongly anionic moiety.⁸² Thus, it tends to form strong bonds with metal ions M^{n+} ($n=1-4$). The phosphonic acid moiety, $R-PO_3H_2$ and its two deprotonated forms, $R-PO_3H^-$ and $R-PO_3^{2-}$ exhibit an interesting, pH-dependent behavior (Figure 14.2). Usually the first proton is very acidic, while the second is a couple orders of magnitude less acidic.^{83–89}

There is a plethora of published crystal structures of “free” (not metal-coordinated) phosphonic acids and their deprotonated forms. It is beyond the scope of this chapter to compile an exhaustive analysis of all the structural features. Only some relevant comments will be made here, that are of significance to the discussion on metal phosphonates.

Polyanchuk *et al.*⁹⁰ have determined the structure of ethylenediamine-tetrakis(methylphosphonic acid) dihydrate, EDTMP (an EDTA analog) from single crystal data (see Figure 14.3). It is worthwhile to have a closer look at the geometrical features of the phosphonate groups.

Due to the high basicity of the N atoms, an internal protonation has occurred. Two protons originating from two diametrically opposite phosphonic acid groups have protonated the N atoms. Hence, the EDTMP molecule is best described as a zwitter-ion with two phosphonic acid groups and two monoprotonated phosphonate groups. The P–O bond distances in the two phosphonic acid groups (P(2) will be used as the example) are 1.529(3) Å, 1.547(3) Å, and 1.476(3) Å, i.e. two “long” and one “short” bond lengths. It is obvious that the “short” bond, 1.476(3) Å, belongs to the P=O phosphoryl group, and the two “long” bonds to the two P–O(H) groups. Similarly, the P–O bond distances in the two monoprotonated phosphonate groups (P(1) will be used as the example) are 1.557(3) Å, 1.486(3) Å, and 1.507(3) Å, i.e. one “long”, one “short”, and one “intermediate” bond lengths. Again, the “short” bond, 1.486(3) Å, belongs to the P=O phosphoryl group, and the “long” bond,

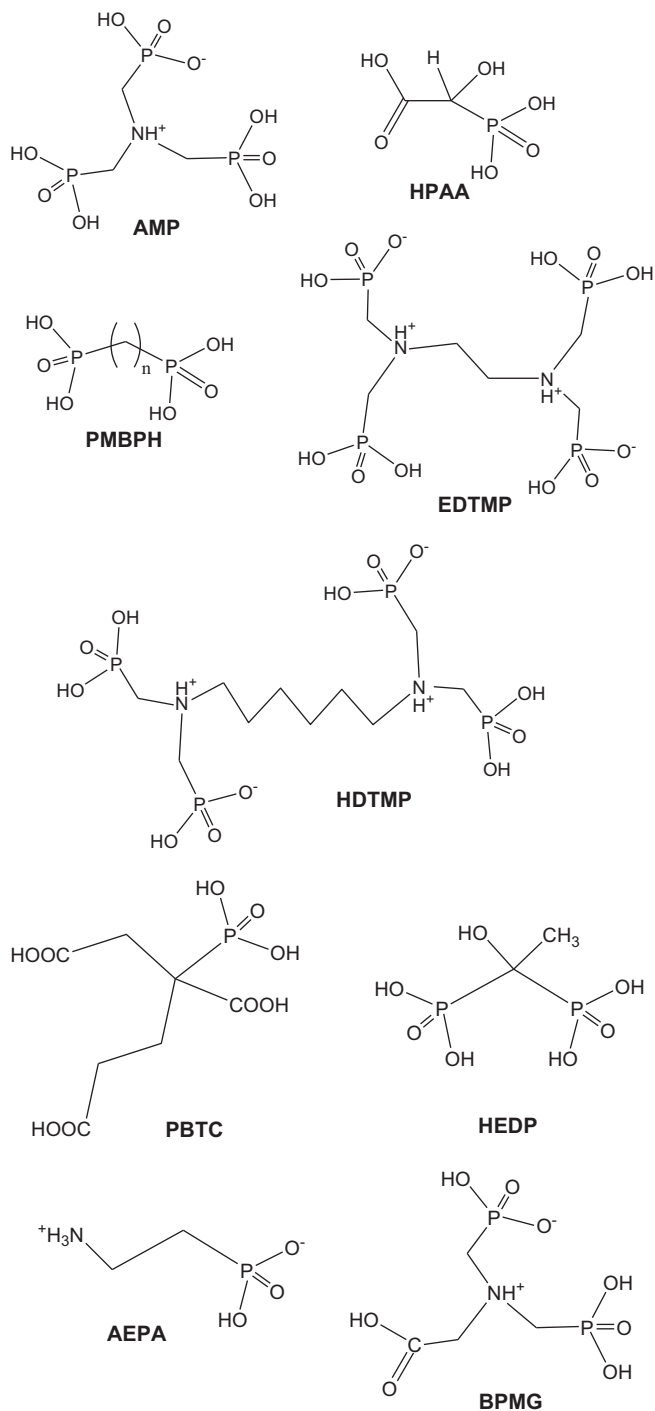


Figure 14.1 Schematic structures of several mono- and poly-phosphonic acids.

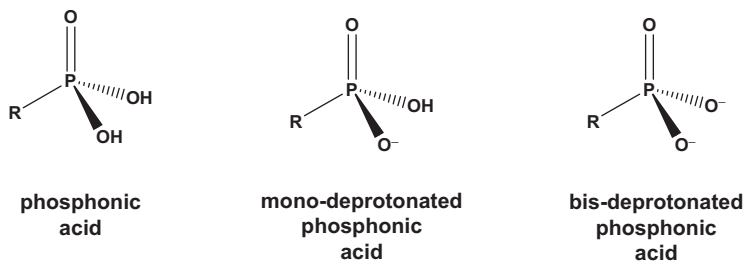


Figure 14.2 The three forms of the phosphonic acid group.

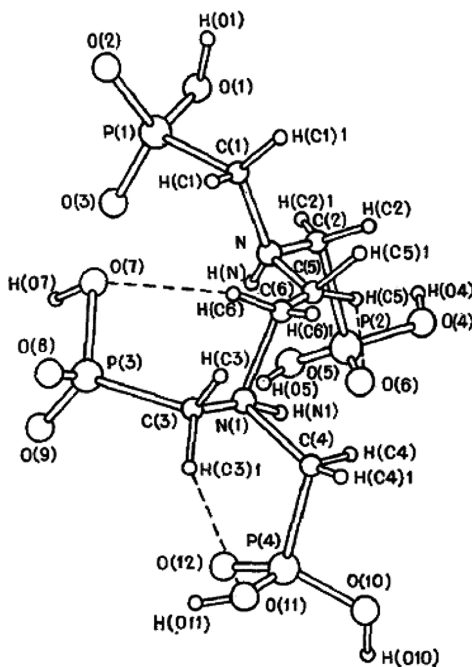


Figure 14.3 The crystal structure of EDTMP dihydrate. (Reproduced with permission from ref. 90.)

1.557(3) Å, to the P–O(H) group. It is therefore reasonable to assume that the “intermediate” bond length be assigned to the monoprotonated –P–O⁻ moiety. The same observations can be noted for the three phosphonic acid groups in the structures of benzene-1,3,5-triphosphonic acid (Figure 14.4),⁹¹ 1,3,5,7-tetrakis(4-phosphonophenyl)adamantane (Figure 14.5),⁹² and 1,2,4-phosphobutane tricarboxylic acid monohydrate (Figure 14.6).⁹³

The same observations can be noted for the monoprotonated phosphonate groups in the ionic tetraphosphonate structures of (en)(HDTMP), (NH₄)(EDTMP), Zn(H₂O)₆(TDTMP) (en = ethylenediamine, see Figure 14.1 for phosphonate names and structures).⁹⁴

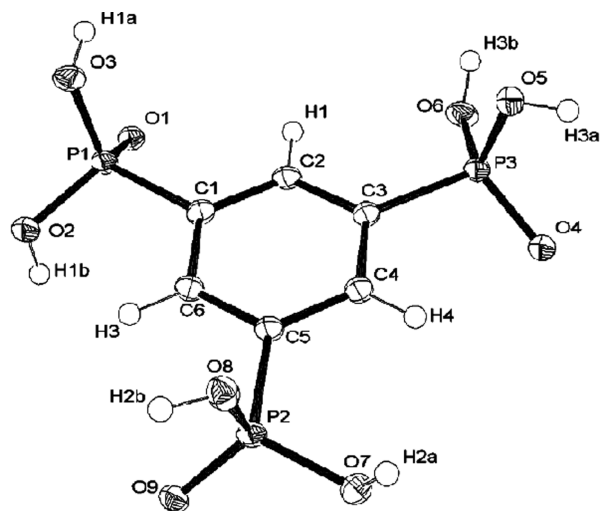


Figure 14.4 The molecular structure of benzene-1,3,5-triphosphonic acid. (Reproduced with permission from ref. 91.)

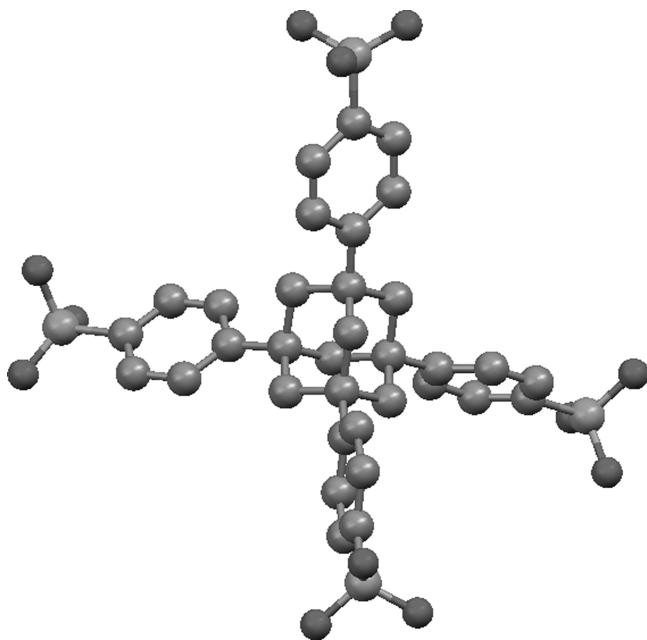


Figure 14.5 The molecular structure of 1,3,5,7-tetrakis(4-phosphonophenyl)adamantane. (Reproduced with permission from ref. 92.)

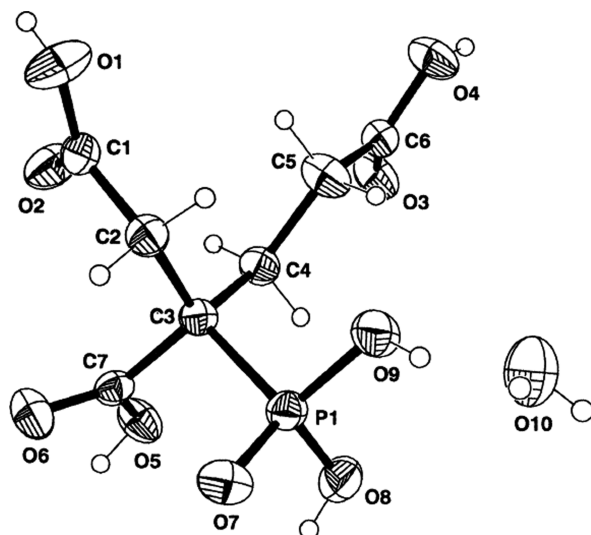


Figure 14.6 The molecular structure of 1,2,4-tricarboxylic acid monohydrate. (Reproduced with permission from ref. 93.)

Upon coordination of the phosphonate oxygens with a metal ion there are a number of structural changes related to the P–O bond lengths. We will demonstrate this by using a number of examples, starting with 1D $[\text{Cu}(\text{HO}_3\text{PCH}(\text{OH})\text{CO}_2)(\text{H}_2\text{O})_2] \cdot \text{H}_2\text{O}$, Figure 14.7.⁹⁵ This material possesses a monodeprotonated phosphonic acid group that is coordinated to a metal ion in a monodentate fashion. The three P–O bond lengths are P(1)–O(4) 1.4931(18) Å, P(1)–O(6) 1.5212(18) Å, P(1)–O(5) 1.5664(19) Å. It is obvious that the 1.5664(19) Å bond distance belongs to the P–O(H) acid group. The shortest distance, 1.4931(18) Å, is assigned to the P=O groups, whereas the remaining “intermediate” distance, 1.5212(18) Å, is the P–O(Cu) moiety. This situation resembles that of a monoprotonated, but not metal-coordinated $-\text{PO}_3\text{H}^-$ moiety, discussed above.

The AMP ligand (AMP = amino-tris(methylenephosphonate)) in the layered 2D material $[\text{Ca}(\text{AMP})(\text{H}_2\text{O})] \cdot 3.5\text{H}_2\text{O}$ coordinates to Ca^{2+} in a monodentate fashion, but in one occasion the phosphonate group is terminal and in the second it is bridging (Figure 14.8).⁴³

Focusing on the Ca–O–P–O–Ca moiety, we note the following bond lengths: P(2)–O(5) 1.4942(15) Å, P(2)–O(4), 1.5102(14) Å, P(2)–O(6) 1.5684(15) Å. Again, the longest P–O bond length, 1.5684(15) Å, belongs to the uncoordinated and protonated P–O(H) moiety. However, the other two P–O bond lengths tend to merge. This occurs because the anionic charge is now more effectively delocalized over the Ca–O–P–O–Ca moiety and it becomes almost impossible to distinguish between the P=O and the P–O[−] groups.

In the structure of $\text{Sr}(\text{AMP})$ (which is anhydrous) one of the AMP arms coordinates to two Sr^{2+} centers in a chelating-bridging fashion. The

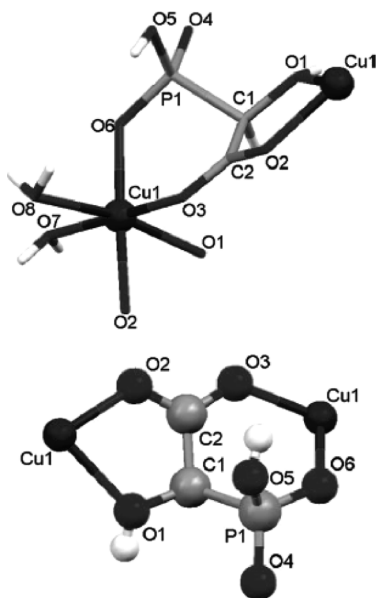


Figure 14.7 Asymmetric unit of $[\text{Cu}(\text{HO}_3\text{PCH}(\text{OH})\text{CO}_2)(\text{H}_2\text{O})_2] \cdot \text{H}_2\text{O}$ (upper) and the ligand chelating/bridging coordination mode (lower). (Reproduced with permission from ref. 95.)

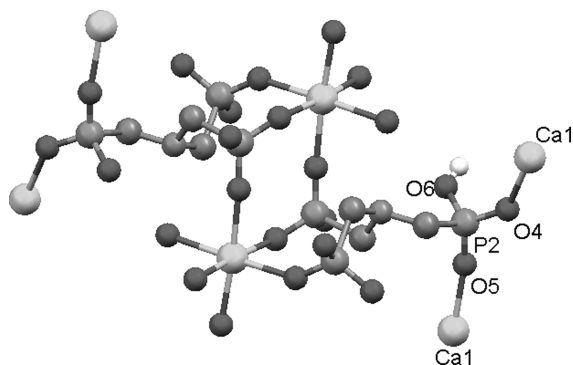


Figure 14.8 Structure of $[\text{Ca}(\text{AMP})(\text{H}_2\text{O})] \cdot 3.5\text{H}_2\text{O}$.

P–O(H) group is not coordinated (Figure 14.9). Similar bond lengths are observed.⁹⁶

In the structure of Ba-AMP the P–O(H) group is now coordinated to a Ba center, creating a 4-membered chelate ring with the P–O group (Figure 14.10).⁹⁶

There are a few examples of metal phosphonate structures in which the mono-deprotonated phosphonic acid group coordinates to three different metal ions.⁹⁷ For instance, in the structure of Ba-CEPA (CEPA = carboxyethylphosphonic acid) a structural motif is observed that is shown in Figure 14.11.

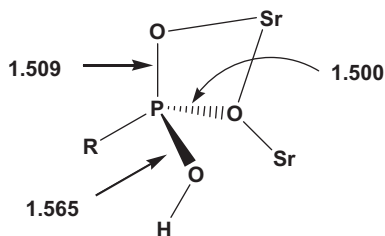


Figure 14.9 Portion of the structure of Sr-AMP. Distances are in Å.

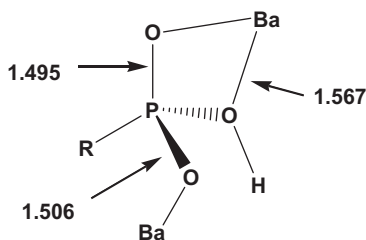


Figure 14.10 Portion of the structure of Ba-AMP. Distances are in Å.

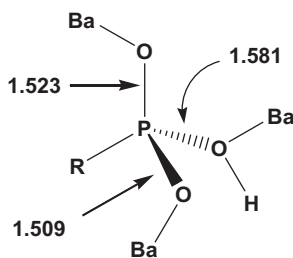


Figure 14.11 Portion of the structure of Ba-CEPA. Distances are in Å.

A slight elongation of all P–O bonds is observed. Still, the P–O(H) bond (although the O is now coordinated to a Ba) is the longest one, 1.581 Å. A similar situation is observed in the structure of Ba-HPAA (HPAA = hydroxyphosphonoacetic acid).^{98,99}

Let us now take a look at the structural changes on the P–O bond lengths when the phosphonate group is doubly deprotonated. In the structures of $[M(\text{phen})_3] \cdot \text{C}_6\text{H}_5\text{PO}_3 \cdot 11\text{H}_2\text{O}$ ($M = \text{Co}, \text{Ni}, \text{Cu}$, phen = 1,10-phenanthroline; Figure 14.12), the phenylphosphonate is found in its doubly deprotonated state, and it is not coordinated.¹⁰⁰

Thus, this is a good example to assess the changes induced in the P–O bond lengths upon complete deprotonation. Thus, the P–O bond lengths are 1.544 Å, 1.497 Å, and 1.505 Å. One of the three P–O bonds (1.544 Å) is still longer than

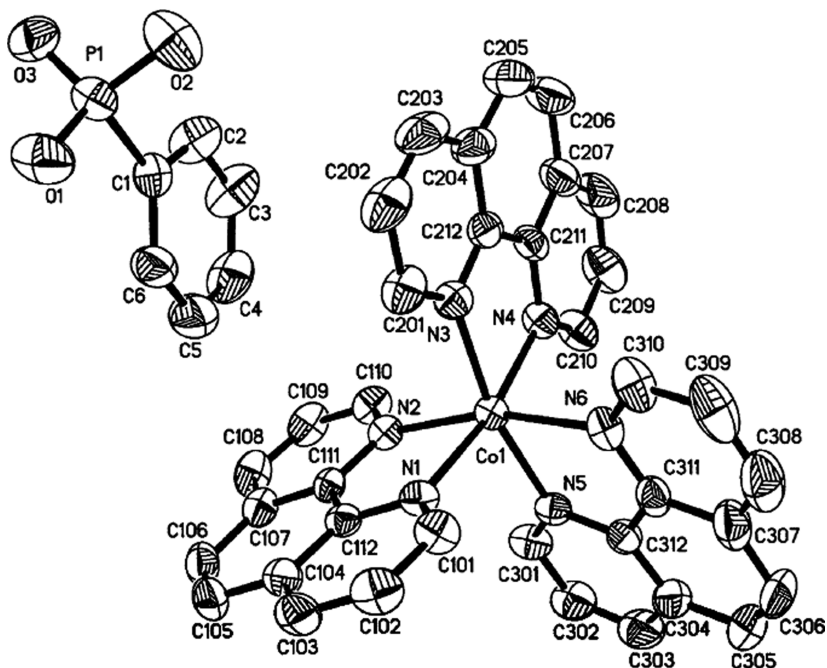


Figure 14.12 The structure of $[M(\text{phen})_3] \cdot \text{C}_6\text{H}_5\text{PO}_3 \cdot 11\text{H}_2\text{O}$. (Reproduced with permission from ref. 100.)

the other two, whose bond lengths tend to merge. It should be noted that the PhPO_3^{2-} dianion participates in an extensive network of hydrogen bonds with the lattice water molecules.

Interaction of strontium acetate with dippH_2 ($\text{dippH}_2 = 2,6\text{-diisopropylphenyl phosphate}$) in methanol at room temperature leads to the isolation of the ionic phosphate $[\{\text{Sr}_2(\mu\text{-H}_2\text{O})_4(\text{H}_2\text{O})_{10}\}\{\text{dipp}\}_2] \cdot 4\text{CH}_3\text{OH}$.¹⁰¹ Interestingly, the P–O bond lengths in the uncoordinated dipp dianion are nearly identical, P1–O1 1.509(7) Å, P1–O2 1.503(6) Å, P1–O3 1.494(6) Å (Figure 14.13).

Upon metal coordination of the doubly deprotonated phosphonic acid group, elongation of the P–O bond lengths is observed. For example, in the structure of $\text{Ba}_2[\text{O}_3\text{P}(\text{CH}_2)_3\text{PO}_3] \cdot 3\text{H}_2\text{O}$ the P–O bond distances are: P(1)–O(3) 1.532(11) Å, P(1)–O(2) 1.536(10) Å, P(1)–O(1) 1.540(10) Å (Figure 14.14).¹⁰²

All phosphonate groups are also deprotonated in the barium phosphonate $[\text{Ba}_3(\text{O}_3\text{PCH}_2\text{NH}_2\text{CH}_2\text{PO}_3)_2(\text{H}_2\text{O})_4] \cdot 3\text{H}_2\text{O}$.¹⁰³ The P–O bond lengths range from 1.507(3) Å to 1.530(3) Å (Figure 14.15).

14.3 The Metal–Oxygen Bond in Metal Coordinated Phosphonates

In this section we will attempt to see whether there are systematic correlations between the oxidation state of the metal ion and the M–O bond distance.

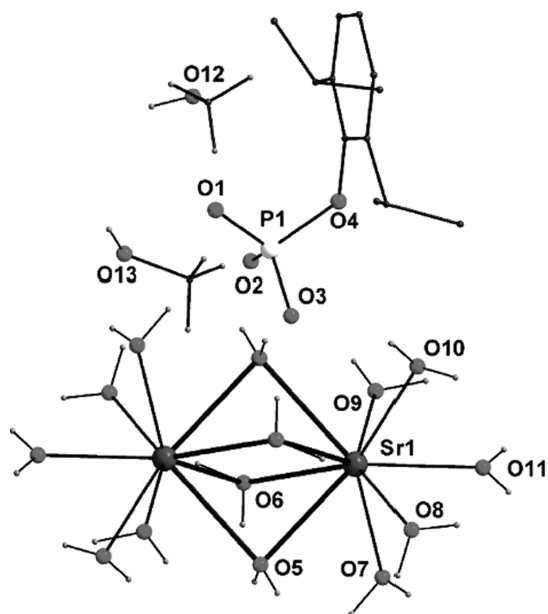


Figure 14.13 The structure of $[\{\text{Sr}_2(\mu\text{-H}_2\text{O})_4(\text{H}_2\text{O})_{10}\}\{\text{dipp}\}_2] \cdot 4\text{CH}_3\text{OH}$. (Reproduced with permission from ref. 101.)

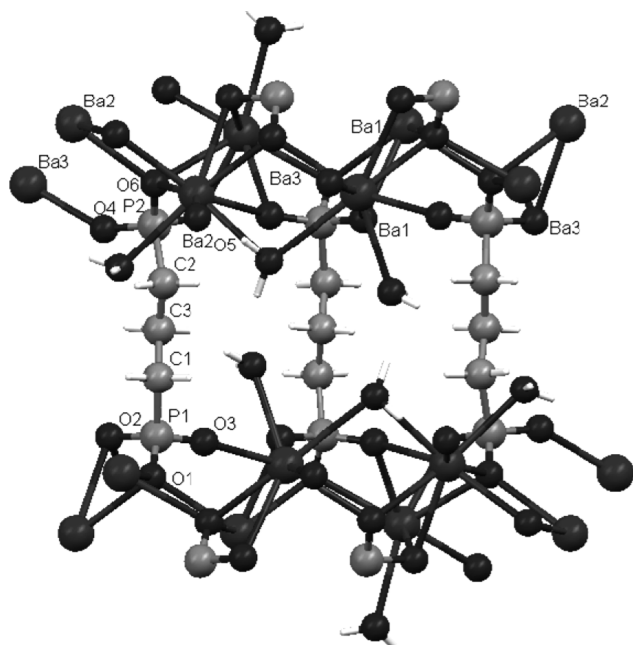


Figure 14.14 The structure of $\text{Ba}_2[\text{O}_3\text{P}(\text{CH}_2)_3\text{PO}_3] \cdot 3\text{H}_2\text{O}$. The diphosphonate ligand acts as a pillar connecting the Ba/O inorganic layer. Structure drawn from the cif file taken from ref. 102.

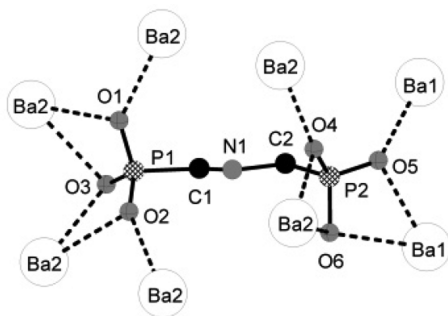


Figure 14.15 The partial structure of $[\text{Ba}_3(\text{O}_3\text{PCH}_2\text{NH}_2\text{CH}_2\text{PO}_3)_2(\text{H}_2\text{O})_4] \cdot 3\text{H}_2\text{O}$, showing the coordination mode of the fully deprotonated phosphonate groups. (Reproduced with permission from ref. 103.)

Correlations are meaningful for metal environments with the same coordination numbers, as a word of caution. The range of Na–O bond distances in the compound Na–N-(phosphonomethyl)glycine is 2.401(2) Å to 2.361(2) Å.¹⁰⁴ Similarly, the Na–O bond distances in the material $\text{Na}_2(\text{AMP}) \cdot 1.5\text{H}_2\text{O}$ range from 2.336(5) Å to 2.489(5) Å.¹⁰⁵ The Li–O bond distances in the compound *catena*-poly[lithium- μ_3 -ethylenediphosphonato] are much shorter, 1.962(4) Å to 1.905(3) Å. This is an indication that the ionic radius plays a significant role, as will be discussed later in this section. It is noteworthy that the P=O bond coordinates to the Li ion, as reported by the authors.¹⁰⁶ Incorporation of a larger monovalent cation in the material $[\text{Ag}_4(\text{O}_3\text{PCH}_2\text{CH}_2\text{PO}_3)]$ creates a wider range of Ag–O bond distances, 2.203(12) Å to 2.530(10) Å.¹⁰⁷ A similar observation can be made for the material Ag–N-(phosphonomethyl)glycine, in which the Ag–O distances are 2.21 Å to 2.53 Å.¹⁰⁴

We will now discuss in a systematic way in the next paragraphs the M–O bond distances, where M = alkaline earth metal cation. It is useful to take a closer look at the M–O bond distances, where M = transition metal cation. A good starting point is the copper phosphonate materials, such as the 1D compound $[\text{Cu}(\text{R},\text{S}\text{-HO}_3\text{PCH}(\text{OH})\text{CO}_2)(\text{H}_2\text{O})_2] \cdot \text{H}_2\text{O}$. The Cu–O distance is 1.9687(18) Å. The phosphonate group is monodentate in this compound.⁹⁵ In a similar material, $\text{Cu}_{1.5}(\text{O}_3\text{PCH}_2\text{CO}_2) \cdot \text{H}_2\text{O}$ (Figure 14.16), the phosphonate group is pentadentate and the Cu–O distances range from 1.909(3) Å to 1.972(3) Å.⁹⁵ It is interesting to note that one of the phosphonate oxygens participates in a Cu– μ_2 -O–Cu bridge; however, the Cu–O distances seem to be unaffected. Lastly, there is a “long” Cu–O distance (2.284(3) Å), but this dramatic elongation is due to the Jahn–Teller effect (common in a d^9 O_h coordination environment).

Similar Cu–O bond distances are noted for the material $\text{Cu}(\text{HO}_3\text{PCH}_2\text{CO}_2) \cdot \text{H}_2\text{O}$.⁹⁵ 1D material $[\text{Cu}(\text{R},\text{S}\text{-HO}_3\text{PCH}(\text{OH})\text{CO}_2)(\text{H}_2\text{O})_2] \cdot \text{H}_2\text{O}$ upon complete dehydration transforms to anhydrous 3D material $\text{Cu}(\text{R},\text{S}\text{-HO}_3\text{PCH}(\text{OH})\text{CO}_2)$, in which the Cu–O bond distances range from 1.994(4) Å to

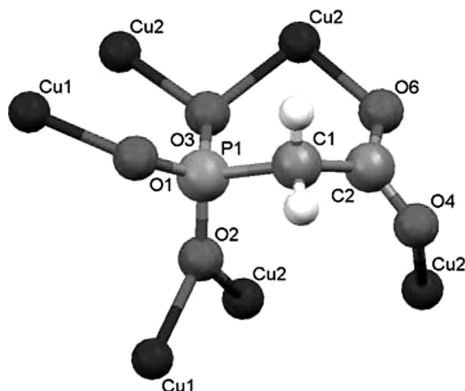


Figure 14.16 Portion of the structure of $\text{Cu}_{1.5}(\text{O}_3\text{PCH}_2\text{CO}_2) \cdot \text{H}_2\text{O}$ that shows the coordination mode of phosphonoacetate. (Reproduced with permission from ref. 95.)

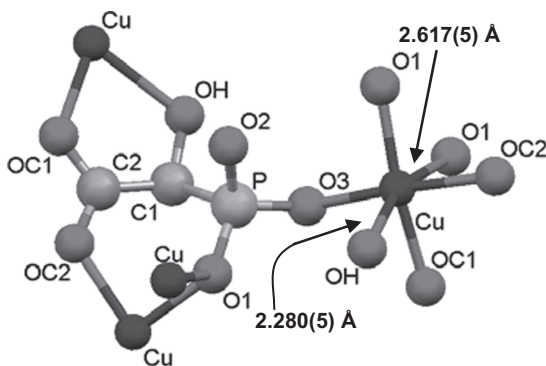


Figure 14.17 Portion of the structure of $[\text{Cu}(\text{R,S-HO}_3\text{PCH}(\text{OH})\text{CO}_2)(\text{H}_2\text{O})_2] \cdot \text{H}_2\text{O}$ that shows the coordination mode of the hydroxyphosphonoacetate. (Reproduced with permission from ref. 108.)

1.988(4) Å (Figure 14.17). As before, there is a long Cu–O distance, 2.617(5) Å, due to the Jahn–Teller effect.¹⁰⁸

1D phases with compositions $[\text{M}\{\text{HO}_3\text{PCH}(\text{OH})\text{CO}_2\}(\text{H}_2\text{O})_2] \cdot 2\text{H}_2\text{O}$ (M = Mg, Co, and Zn) have been isolated.¹⁰⁹ These materials are isostructural. The Zn material and its various hydrated forms display a range of Zn–O distances from 2.042 Å to 2.064 Å. In the molecular Co^{II} phosphonate $[\text{Co}(\text{H}_2\text{O})_6][\text{Co}(\text{H}_2\text{O})_4(\text{HDTMP})_2] \cdot 12\text{H}_2\text{O}$ the Co–O distance is 2.106(2) Å.¹¹⁰ The Co–O bond lengths in the 3D material poly[cesium(I) [μ_4 -ethylenediphosphonato)cobalt(II)]], $\{\text{Cs}[\text{Co}(\text{C}_2\text{H}_5\text{O}_6\text{P}_2)]\}_n$, fall in the range from 1.934(3) Å to 1.965(2) Å. The Co is found in a tetrahedral environment.¹¹¹ These Co–O bond lengths are comparable to those found in other cobalt(II) phosphonates containing Co^{II} in a tetrahedral environment.^{23,112–117}

In 1D linear $[\text{Fe}(\text{H}_2\text{PMIDA})(\text{H}_2\text{O})_2]$ (PMIDA = phosphonomethyl-imino-diacetic acid) there are two Fe–O bond distances, 2.051(2) Å and 2.182(2) Å.¹¹⁸ This paper furnishes useful crystallographic information on Fe–O and Fe–N bond distances, based on statistical analyses of a CSD search. In the 3D material $(\text{NH}_3\text{C}_6\text{H}_4\text{NH}_3)\text{Fe}_2(\text{HEDP}) \cdot 2\text{H}_2\text{O}$, $\text{HEDP} = \text{C}(\text{CH}_3)(\text{OH})(\text{PO}_3)_2^{2-}$, the Fe–O bond distances are 2.050(2) Å to 2.150(2) Å. Here, there seems to be a wide range of bond lengths.¹¹⁹

The 3D material $\text{Mn}[(\text{HO}_3\text{PCH}_2)_2\text{N}(\text{H})(\text{CH}_2)_4(\text{H})\text{N}(\text{CH}_2\text{PO}_3\text{H})_2]$ is built from alternating corner-linked $[\text{MnO}_6]$ and $[\text{PO}_3\text{C}]$ polyhedra forming a 2D net of eight rings. These layers are connected to a pillared structure by the diaminobutane groups. Magnetic susceptibility data confirms the presence of Mn^{2+} ions.¹²⁰ The Mn–O bond distances are in the range 2.138(2)–2.219(2) Å.

In the 2D zigzag material Zn-AMP the Zn–O distances are 2.049 Å and 2.122 Å.¹²¹ In a different, 3D Zn-AMP material, $\text{Zn}_2[\text{HO}_3\text{PCH}_2\text{NH}(\text{CH}_2\text{PO}_3)_2]$, containing tetrahedral Zn centers, the Zn–O bond distance is 1.928(7) Å to 1.964(8) Å.¹²² In Zn-HDTMP the Zn–O distances are in the range 2.022(3)–2.067(3) Å.¹²³ In the 1D Zn-HPAA material the Zn–O distance is 2.042(2) Å.¹⁰⁹

In the 1D material Ni-HPAA the Ni–O distance is 2.0322(18) Å.¹²⁴

In the chromium(II) methyl phosphonate dihydrate, $[\text{Cr}(\text{CH}_3\text{PO}_3)(\text{H}_2\text{O})] \cdot \text{H}_2\text{O}$, the Cr–O bond distances are 2.031 Å, and there is a “longer” one corresponding to a μ_2 -O phosphonate, of 2.084 Å.¹²⁵ Similar distances are reported for the organometallic Cr^{II} phosphonate $[\eta^6\text{-}1,2\text{-C}_6\text{H}_4(\text{OCH}_3)(\text{P}(\text{O})(\text{OCH}_2\text{CH}_3)_2)]\text{Cr}(\text{CO})_3$.¹²⁶

In Al-AMP phosphonate material, $\text{Al}[(\text{HO}_3\text{PCH}_2)_3\text{N}] \cdot \text{H}_2\text{O}$, the Al–O bond distances were reported to be in the range 1.841(14) Å to 2.011(14) Å.¹²⁷ In the framework of $\text{Al}^{\text{III}}\text{-}N,N'$ -piperazinebis(methylenephosphonate) the Al–O bond distances are 1.98(2) Å and 2.05(2) Å.³⁵ The Al–O bond distances in the layered phosphonate $\text{Al}(\text{OH})(\text{O}_3\text{PCH}_3) \cdot \text{H}_2\text{O}$ are in a “tighter” range 1.870(1) Å to 1.881(1) Å.¹²⁸ Similarly, the Al–O distances in the material $(\text{C}_5\text{H}_5\text{NH})\{\text{AlF}[\text{O}_3\text{PCH}_2\text{PO}_2(\text{OH})]\} \cdot 0.61\text{H}_2\text{O}$ fall into the range 1.876(3) Å to 1.898(2) Å.¹²⁹ For Fe^{III} phosphonates, the Fe–O distances are a bit longer than the corresponding Al–O ones. For example, in the iron diphosphonate $\text{Fe}^{\text{III}}(\text{HO}_3\text{PCH}_2\text{CH}_2\text{PO}_3)(\text{H}_2\text{O})$ the Fe–O distances range from 1.980(3) Å to 1.989(3) Å.¹⁹ Similar Fe–O distances are observed in $[\text{Fe}_4\text{O}(t\text{-BuPO}_3)_3(\text{O}_2\text{CPh})_3(\text{py})_3\text{Cl}] \cdot 3.5\text{py}$ (py = pyridine), 1.913(9) Å to 1.964(5) Å.¹³⁰

In the framework of $\text{Ti}^{\text{IV}}\text{-}N,N'$ -piperazinebis(methylenephosphonate) (MIL-91(Ti)) the Ti–O bond distances are 2.16(2) Å, 2.01(2) Å.³⁵ In the “mixed” Sn^{IV} oxalate/methylphosphonate material $\text{Sn}_2(\text{O}_3\text{PCH}_3)(\text{C}_2\text{O}_4)$ a Sn–O bond distance of 2.092 Å has been noted.¹³¹ Contrast this to a Sn^{II} compound, tin(II)-phenylbis(phosphonate), $\text{Sn}_2(\text{O}_3\text{PC}_6\text{H}_4\text{PO}_3)$, where the Sn–O distances are only a bit longer, 2.095(4) Å to 2.145(2) Å.¹³² Another Sn^{II} polymeric compound, poly[tin(II)- μ -phenylphosphonato], $[\text{Sn}(\text{C}_6\text{H}_5\text{O}_3\text{P})]_n$, shows a Sn–O distance range of 2.097(3) Å to 2.133(3) Å.¹³³ Similarly, the Sn–O distances in the Sn^{II} compound $\text{Sn}_2[\text{O}_3\text{PCH}_2\text{C}_6\text{H}_4\text{CH}_2\text{PO}_3]$, are 2.11(1) Å to 2.19(1) Å.¹³⁴

The reader is referred to Chapter 9, which describes in detail structural aspects of Zr-phosphonate chemistry. Only a few representative examples will be mentioned here. In the linear chain zirconium organophosphonate $(\text{NH}_4)\text{Zr}[\text{F}_2][\text{H}_3\{\text{O}_3\text{PCH}_2\text{NH}(\text{CH}_2\text{CO}_2)_2\}_2] \cdot 3\text{H}_2\text{O} \cdot \text{NH}_4\text{Cl}$, the Zr–O bonds are found in the range 2.058(2) Å to 2.092(2) Å.¹³⁵

Interestingly, the Zr–O distances in the compound $\text{Zr}_2(\text{O}_3\text{PCH}_2\text{CH}_2\text{-bipyridinium-CH}_2\text{-CH}_2\text{PO}_3)\text{-F}_6\text{-}2\text{H}_2\text{O}$ are slightly longer, 2.130(7) Å to 2.157(6) Å.¹³⁶ In a similar compound, $\text{Zr}_2(\text{O}_3\text{PCH}_2\text{CH}_2\text{-viologen-CH}_2\text{CH}_2\text{PO}_3)\text{F}_6 \cdot 2\text{H}_2\text{O}$, the Zr–O distances are from 2.03(1) Å to 2.09(1) Å.¹³⁷ Similar Zr–O distances are noted for the zirconium diphosphonate fluoride, $\text{ZrHF}(\text{O}_3\text{PCH}_2)_2\text{NHC}_3\text{H}_6\text{CO}_2$ that contains the 4-[bis(phosphonomethyl)amino]butanoic acid ligand, 2.01(1) Å to 2.16(1) Å.¹³⁸ Additionally, the Zr–O distances in $\text{ZrF}(\text{O}_3\text{PCH}_2)_2\text{NHCH}_2\text{C}_6\text{H}_5$ fall in the range 2.051(7) Å to 2.112(6) Å.¹³⁹ The layered zirconium chloromethylphosphonate, $\text{Zr}(\text{O}_3\text{PCH}_2\text{Cl})_2$, displays Zr–O distances from 1.991(8) Å to 2.085(8) Å.¹⁴⁰ Recently, two interesting Zr^{IV} tetraphosphonate compounds were reported, $\text{Zr}(\text{HPO}_3\text{CH}_2)_2\text{N-C}_4\text{H}_8\text{-N}(\text{CH}_2\text{PO}_3\text{H})_2 \cdot 4\text{H}_2\text{O}$ and $\text{Zr}(\text{O}_3\text{PCH}_2)_2\text{N-C}_6\text{H}_{10}\text{-N}(\text{CH}_2\text{PO}_3)_2\text{Na}_2\text{H}_2 \cdot 5\text{H}_2\text{O}$, in which the Zr–O distances fall in the ranges 2.093–2.119 Å (for the former) and 2.014–2.083 Å (for the latter).⁴¹ Similar Zr–O distances were reported for a family of layered diphosphonate compounds, $\text{ZrF}(\text{O}_3\text{PCH}_2)_2\text{NHC}_n\text{H}_{2n+1}$ ($n = 1\text{--}10$).⁴²

The previous examples point to an interesting observation, that there are no systematic trends between the metal ion oxidation state and the M–O bond distance. Therefore, it will be informative to seek similar trends between the metal ion ionic radius and the M–O bond distance.

Our discussion on the effect of the metal ionic radius on the M–O bond distance will focus on divalent metal ions, for the convenience of comparisons and also due to the plethora of divalent metal phosphonate structures. A good starting example is the series of M-AMP materials (M = Mg, Ca, Sr, Ba). Apparently, there is a steady increase of the M–O bond distance as the metal ion increases in size.^{43,96} This is clearly shown in Figure 14.18, where M–O bond distances (shortest and longest) are plotted versus the ionic radii.

An identical trend is observed for the series M-HPAA materials (M = Mg, Ca, Sr, Ba), as shown in Figure 14.19.^{98,99,109}

Bond distances versus ionic radii of the first row divalent transition metal ions are plotted in Figure 14.20. It is obvious that there is no discernible trend.

In contrast, there is a clear trend in the M–O bond distances, when M is a monovalent alkali metal ion (Figure 14.21). M–O bond distances were taken from references 106 (Li), 104 (Na), 109 (K), 141 (Rb), and 97 (Cs).

14.4 Metal–Phosphonate versus Metal–Carboxylate Bonding

Among the battery of anionic ligands available for the construction of inorganic–organic hybrids, polycarboxylates are predominant.^{142–150}

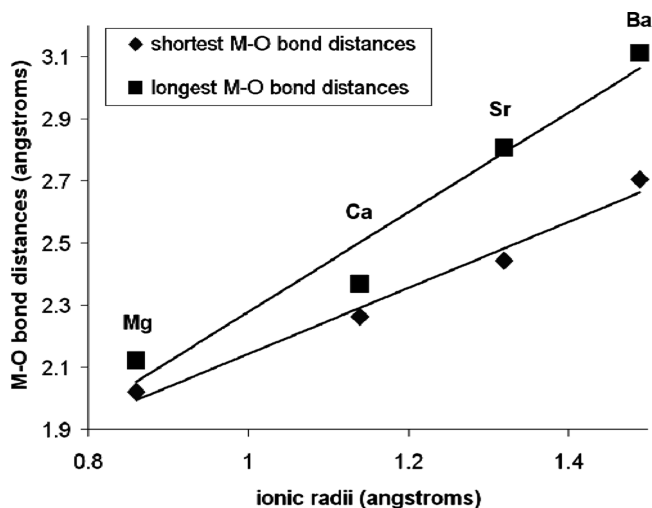


Figure 14.18 Correlation of M–O bond distances (M = Mg, Ca, Sr, and Ba) with the corresponding ionic radii in a series of metal-AMP hybrids.

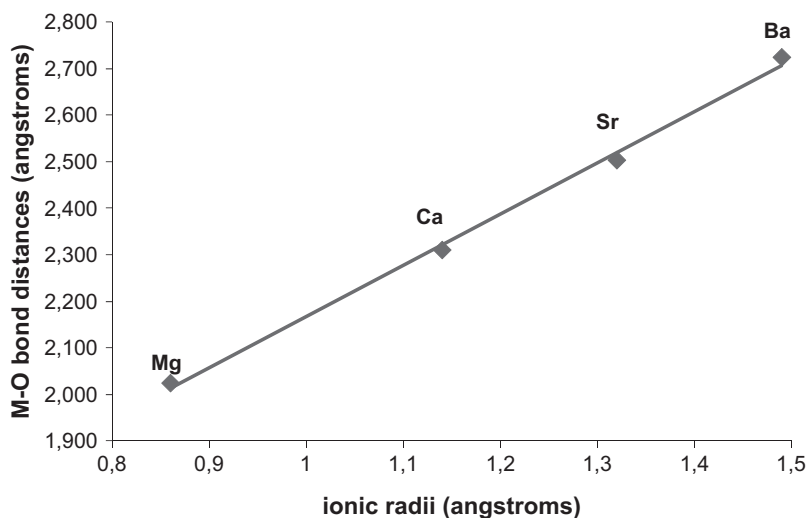


Figure 14.19 Correlation of M–O bond distances (M = Mg, Ca, Sr, and Ba) with the corresponding ionic radii in a series of metal-HPAA hybrids.

Polyphosphonates have also attracted significant interest,^{3,6,40,64} because they exhibit a number of similarities, but also differences, to the carboxylates.

- (a) Phosphonate building blocks possess three O atoms linked to the phosphorus atom in the coordinating moiety, compared to two O atoms in the

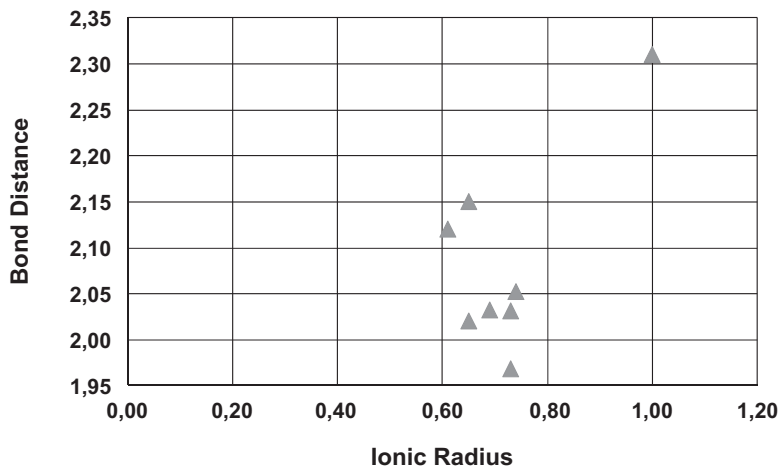


Figure 14.20 Correlation of M–O bond distances (M = first row divalent transition metal ions) with the corresponding ionic radii in a various metal(II)-phosphonate hybrids.

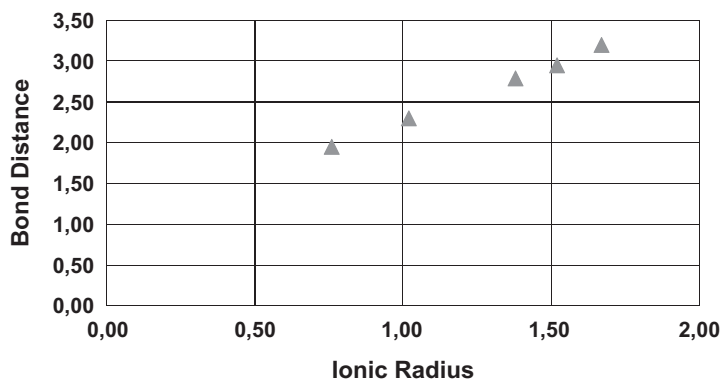


Figure 14.21 Correlation of M–O bond distances (M = alkali metal ions) with the corresponding ionic radii in a various metal(I)-phosphonate hybrids.

case of carboxylates. This increases the possibilities for access to novel structures.

- (b) The phosphonic acid moiety can be doubly deprotonated in two well-defined successive steps, depending on solution pH.⁸² Carboxylic acid ligands can only be deprotonated once (Figure 14.22). Again, this allows access to a variety of potential novel phosphonate-containing structures, by simply varying the pH.
- (c) The phosphonate group can be (potentially) doubly esterified, in contrast to the carboxylate group that can only be monoesterified.^{151–154} Introduction of at least one phosphonate ester in the building block is expected

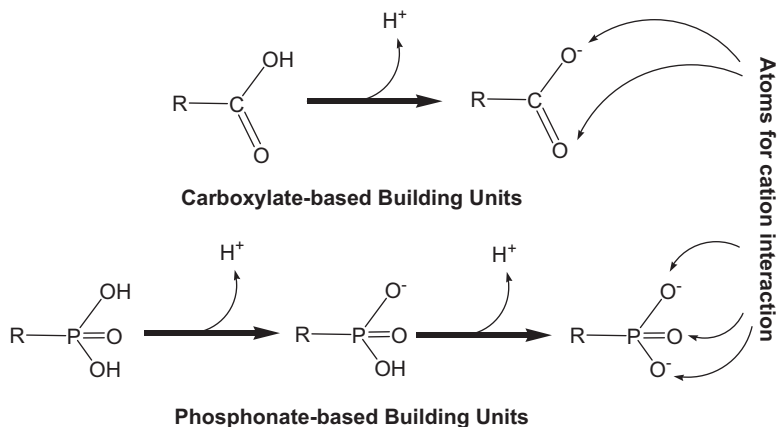


Figure 14.22 Structural and functional differences between carboxylic and phosphonic acids.

to enhance solubility (in the case of very insoluble materials), or by virtue of its hydrolysis,⁹⁵ to yield structural diversity in the end material.

- (d) Synthesis of metal phosphonate materials can be carried out via a number of different routes that do not necessarily give products with the same structure. There is hence a greater potential of structural diversity in the products derived. Several of these methods lend themselves to a combinatorial approach allowing high-throughput screening of candidate materials to be achieved.²⁸ In this context, a recent review was published on “non-carboxylate” MOFs.¹⁵⁵

14.5 Synthetic Considerations

14.5.1 pH

Recently, an important review was published on the effect of pH on the assembly of metal–organic architectures.¹⁵⁶ It is clear that pH plays an important role in determining the final structures of the inorganic–organic hybrids. Significant progress has been made in synthetic endeavors; however, it appears that prediction of any specific effects caused by pH changes remains elusive. Such effects are unknown *a priori*, and there is often more than one effect that comes into play, resulting in complex and diverse structures of such materials. Furthermore, the assembly of the solid state structures of such architectures is governed by a number of intermolecular forces in addition to the pH influence. Frequently, the balance between said forces is so subtle that a convincing explanation of some structures observed is argumentative. An example experienced in our laboratories is the formation of two Sr-HPAA materials, namely $Sr[(HPAA)(H_2O)_3] \cdot H_2O$ and $Sr(HPAA)(H_2O)_2$.^{98,99} These two materials are synthesized under identical conditions, except that the former

forms at pH 2.0, whereas the latter forms at pH 2.7. Further progress and a deeper understanding of the diverse effects of pH on synthesis depend on further systematic studies. For instance, isolation of possible intermediates should provide useful insight. Computational studies should also shed some light on possible pH effects. Combined, the results of experimental and computational studies will allow further and more thoughtful design in the context of crystal engineering with the goal of gaining access to structurally and functionally more sophisticated and useful materials.^{157–160}

14.5.2 Temperature

It has been noted that by changing the reaction conditions, it is sometimes possible to synthesize a number of different materials from the same combination of metal salt and phosphonate anion. Examples include the families of aluminum phenylphosphonates and benzylphosphonates reported by Cabeza¹⁶¹ and Zakowsky,²⁶ respectively, and the copper methylphosphonates reported by Bujoli.¹⁶² It is quite common that different products are formed from a particular set of reagents have the different compositions, and are not polymorphs of one another. More often the materials will contain different metal:phosphonate ratios, arising from charge variations on the phosphonate anion backbone, which, in turn, are dependent on reaction mixture pH. Other variations include the number of water molecules (either metal-coordinated or in the lattice) in the structure. This is often a result of differences in the coordination number, environment of the metal atoms, and hydrogen bonding schemes.

The hydrothermal synthetic procedure was carried out using different Cu:P ratios and at different temperatures.⁹⁵ Figure 14.23 shows which products are obtained from each of the Cu:P ratios used at the different reaction temperatures.

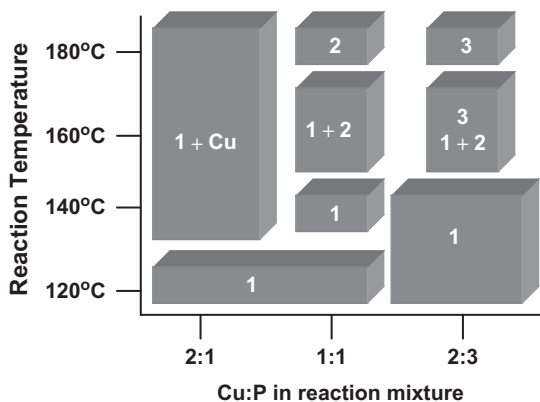


Figure 14.23 Products formed from reactions between copper acetate and diethylphosphonoacetic acid, under hydrothermal conditions at different temperatures and with varying reactant ratios. α - $\text{Cu}_{1.5}(\text{O}_3\text{PCH}_2\text{CO}_2) \cdot \text{H}_2\text{O}$ (1), β - $\text{Cu}_{1.5}(\text{O}_3\text{PCH}_2\text{CO}_2) \cdot \text{H}_2\text{O}$ (2), $\text{Cu}(\text{HO}_3\text{PCH}_2\text{CO}_2) \cdot \text{H}_2\text{O}$ (3). (Reproduced with permission from ref. 95.)

The initial experiment carried out in the investigation of this system was carried out using a 1:1 mole ratio of copper acetate to DPAA (or Cu:P ratio) at 160 °C. The products appeared to consist of three phases; large dark green block crystals, large bright blue plates, and small turquoise plates. Crystals were separated by hand and investigated by single crystal methods, which showed the bright blue and turquoise materials to be the same phase. Hence the products of this reaction are biphasic, with both phases having a composition of $\text{Cu}_{1.5}(\text{O}_3\text{PCH}_2\text{CO}_2) \cdot \text{H}_2\text{O}$, but with different structures (see below).

Treatment of the 1:1 Cu:P reaction mixture at 140 °C resulted in the formation of the blue material (hereafter referred to as the α -phase) as a single phase product. Another single crystal measurement was carried out on this material, confirming it to be identical to the blue phase obtained at 160 °C. The single phase nature of this material was confirmed by comparison of an observed powder X-ray diffraction pattern with one generated from the single crystal data. The same result was obtained for a synthesis carried out at 120 °C. Isolation of the material as a single phase allowed CHN analyses to be carried out. These results confirmed the elemental composition determined during the single crystal analysis.

Treatment of the same 1:1 reaction mixture at 180 °C results in the formation, as a single phase product, of the green phase obtained at 160 °C. Again this was confirmed by additional single crystal analysis and comparison with powder diffraction patterns. CHN analysis confirms the composition of the β -phase to be the same as that of the α -phase and corresponds to the stoichiometry obtained from the single crystal analysis.

Treatment of a reaction mixture with a Cu:P ratio of 2:3 (taking into account the stoichiometry of the previously obtained products) at 160 °C again gave rise to a mixture of products. In this case however, the products contained, $\text{Cu}_{1.5}(\text{O}_3\text{PCH}_2\text{CO}_2) \cdot \text{H}_2\text{O}$ (**1**), $\text{Cu}_{1.5}(\text{O}_3\text{PCH}_2\text{CO}_2) \cdot \text{H}_2\text{O}$ (**2**) and bright blue, block shaped crystals. Single crystal analysis of the new product (see below) showed the product to have a composition of $\text{Cu}(\text{HO}_3\text{PCH}_2\text{CO}_2) \cdot \text{H}_2\text{O}$ (**3**). When the reaction temperature was raised to 180 °C this material was obtained as a single phase, allowing a CHN analysis to be carried out, and again confirming the composition determined from the single crystal analysis. Using the same 2:3 Cu:P reactant ratio at a reaction temperature of 140 °C or below results in the formation of **1** only.

A further change in the relative amounts of the starting reagents such that the Cu:P ratio was 2:1 did not yield any new materials. At temperatures of 140 °C and above, the hydrothermal reaction gave rise to a mixture of copper metal and **1**. The quantity of copper metal obtained increased as the reaction temperature was raised.

14.6 Auxiliary Ligands

A secondary ligand is occasionally introduced into the synthesis mixture in the hope of gaining access to novel products. There are cases where this ligand (often an amine-based molecule) acts as a template for the formation of end

products. There are cases reported where this ligand ends up in the final structure. For example, $(\text{NH}_4)\text{Zn}[\text{O}_3\text{PCH}(\text{OH})\text{CO}_2]$ forms from a mixture of zinc acetate, NH_4Cl , and HPAA in water (final pH 4.12) at 190°C .¹⁶³

Often, the auxiliary ligands used are bidentate chelates, such as 2,2'-bpy or 1,10-phen, although there are reports of 4,4'-bpy utilization as a bridge. The reaction of copper acetate with phosphonoacetic acid in the presence of phen yields a binuclear complex in which phen acts as a chelating ligand, whereas the two Cu ions are bridged by two phosphonoacetate ligands.¹⁶⁴ Two pillared metal phosphonates, $[\text{Mn}_3(4,4'\text{-bpy})(\text{HPAA})_2] \cdot (4,4'\text{-bpy})_{0.5}$ and $[\text{Co}_3(4,4'\text{-bpy})(\text{H}_2\text{O})_2(\text{HPAA})_2] \cdot (4,4'\text{-bpy})_{0.5}$ have been synthesized hydrothermally, and structurally characterized. The Mn^{II} and Co^{II} ions are found in octahedral coordination environment and bridged by the HPAA ligand through $-\text{OH}$, $-\text{COO}$ and $-\text{PO}_3$ groups into a hybrid layer. The layers are further pillared by the coordinated 4,4'-bpy into a 3D neutral framework.¹⁶⁵ In the presence of ethylenediamine template agents, a Fe^{II} phosphonate, $[\text{NH}_3\text{CH}_2\text{CH}_2\text{NH}_3][\text{Fe}_2(\text{HPAA})_2(\text{H}_2\text{O})_2] \cdot 2\text{H}_2\text{O}$ has been synthesized under hydrothermal conditions and characterized by single-crystal X-ray diffraction.¹⁶⁶ The Fe^{II} cation is octahedrally coordinated by six oxygen atoms from the three ligands and one coordinated water molecule to form a 2D layered structure with a 1D channel system in the a axis direction. In this case ethylenediamine does not coordinate to the Fe^{II} . A new Co^{II} phosphonate, $[\text{NH}_3\text{CH}_2\text{CH}_2\text{NH}_3]_{0.5}[\text{Co}(\text{HPAA})(\text{H}_2\text{O})] \cdot \text{H}_2\text{O}$, has been hydrothermally synthesized and structurally characterized. It has a honeycomb-like layer structure which is composed of CoO_6 octahedra and μ_3 -HPAA ligands with the protonated ethylenediamine and lattice water molecules stabilized between the layers. As before, the ethylenediamine does not coordinate to the Co^{II} .¹⁶⁷ In the presence of ethylenediamine, a layered antimony(III) phosphonate, $[\text{NH}_2\text{CH}_2\text{CH}_2\text{NH}_2][\text{Sb}_2(\text{HPAA})_2]$ has been synthesized by hydrothermal reaction at 140°C and characterized by single-crystal X-ray diffraction.¹⁶⁸ In this case, although the ethylenediamine is not protonated in the crystal lattice, it does not coordinate to the Sb^{III} . Two new metal phosphonatobenzenesulfonates using 1,10-phenanthroline as auxiliary ligand, namely, $[\text{Cu}(\text{HL})(\text{phen})] \cdot 0.5\text{H}_2\text{O}$ and $[\text{Y}(\text{L})(\text{phen})(\text{H}_2\text{O})_2] \cdot 2\text{H}_2\text{O}$ ($\text{H}_3\text{L} = m\text{-HO}_3\text{S-C}_6\text{H}_4\text{-PO}_3\text{H}_2$, phen = 1,10-phenanthroline), have been synthesized by hydrothermal reactions.¹⁶⁹ Both compounds feature 1D chain-like structures. The 1D chain structure in the first features $\text{Cu}_2(\text{PO}_3)_2$ dimers fused by the bridging of pairs of bidentate phosphonate groups, which are further interconnected via pairs of monodentate sulfonate groups. In contrast, the 1D chain in the latter features an edge-shared four-membered ring which is composed of two Y^{III} ions and two tridentate phosphonate groups. The different 1D chain structures in them are mainly due to the various coordination modes of the 3-phosphonobenzenesulfonic acid ligand. The reaction of copper perchlorate with monophosphonic acids of the type RPO_3H_2 ($\text{R} = \text{cyclopentyl}$, isopropyl, trichloromethyl) in the presence of chelating nitrogen ligands bpya (bpya = 2,2-bipyridylamine) or bpy afforded dinuclear copper phosphonates that feature the $[\text{Cu}_2(\mu_2\text{-RPO}_3)_2]$ core.¹⁷⁰ Similar reaction with copper salts and monophosphonates in the presence of phen and acetic acid yield higher nuclearity clusters, such as $[\text{Cu}_4(\mu\text{-CH}_3\text{COO})_2(\mu_3\text{-C}_6\text{H}_{11}\text{PO}_3)_2(2,2'\text{-bpy})_4](\text{CH}_3\text{COO})_2$.¹⁷¹

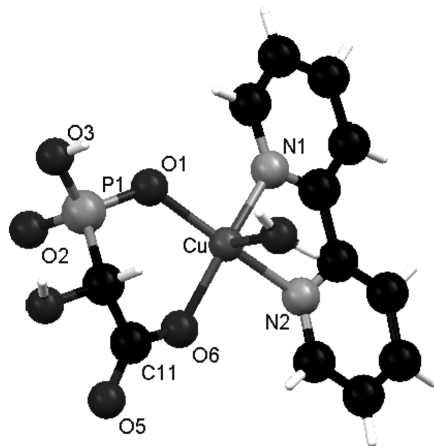


Figure 14.24 The molecular structure of the mononuclear complex, $[\text{Cu}(\text{R},\text{S}\text{-HO}_3\text{P}\text{-CH}(\text{OH})\text{CO}_2)(\text{bpy})(\text{H}_2\text{O})] \cdot \text{H}_2\text{O}$. The lattice water has been omitted for clarity.

In an effort to diverge the synthesis end material from $[\text{Cu}(\text{R},\text{S}\text{-HO}_3\text{P}\text{-CH}(\text{OH})\text{CO}_2)(\text{H}_2\text{O})_2] \cdot \text{H}_2\text{O}$, we utilized bpy in the reaction mixture. The end product was a mononuclear complex, $[\text{Cu}(\text{R},\text{S}\text{-HO}_3\text{P}\text{-CH}(\text{OH})\text{CO}_2)(\text{bpy})(\text{H}_2\text{O})] \cdot \text{H}_2\text{O}$ (Figure 14.24).¹⁷²

Chapter 5 in this book offers an in-depth discussion on metal phosphonate materials that contain an auxiliary ligand.

14.7 Applications

Organophosphonate anions (see Figure 14.1) function as linkers connecting inorganic centers to yield hybrid frameworks. Tailored design of the linker molecules is easy because phosphonic acids are prepared in relatively simple procedures, or occasionally are commercially available. Chemical and thermal stability of phosphorus–carbon bonds in phosphonates is considered to be high. Generally, metal phosphonate solids are prepared either at room temperature or under mild hydrothermal conditions. Such experimental conditions cause little or no decomposition of organic moieties in several cases. Therefore, phosphonates are suitable to design inorganic–organic nano-hybrid materials. Such merits of phosphonates have been recognized for layered materials since Alberti and co-workers reported the first metal phosphonate in 1978.¹⁷³ Structural similarities between metal organophosphonates and the corresponding phosphates were revealed through studies on layered phosphonates¹⁷⁴ and tailored design of the materials became subsequently possible. A detailed review on metal phosphonate materials by Clearfield is available,⁵ along with reviews on layered metal phosphonates and their use.^{175,176}

During the last decade, possibilities of incorporating organic molecules into ordered nanoporous inorganic solids were extensively explored. As surveyed in

a review by Maeda,¹⁷⁷ organically modified mesoporous silicas were realized both by post-modification of the purely inorganic materials using organosilylation agents and by direct incorporation of organosiloxane during assembly of silicate frameworks. When these approaches are applied for microporous materials, however, the post-modification has difficulties in leaving accessible pores owing to their much smaller pore sizes. Direct crystallization needs careful selection of a suitable system. For example in the silicate system, partial substitution of the framework oxygen atoms in several known zeolite structures by methylene groups was attained recently.¹⁷⁸ Considerable parts of the Si–C bond of methylene-bridged organosilane used as the silicon source, however, were cleaved under strongly basic hydrothermal conditions. Thus, chemical and thermal stabilities of organophosphonic acids and moderately mild synthetic conditions of metal phosphonates tempted many researchers to explore open-framework solids. Structural and chemical properties of metal phosphonates are variable depending on many synthetic parameters such as phosphonate source, metal source, metal/P ratio, solvent, concentration, pH, and reaction temperature.

In the following sections we will discuss several properties and applications of metal phosphonates and we will make an attempt to correlate structure with function.

14.8 Corrosion Protection by Metal Phosphonate Thin Film Formation

Corrosion is a wide and highly interdisciplinary field of science. Corrosion inhibition by chemical means (i.e. with the use of corrosion inhibitors) is a significant part of corrosion science, whose scientific literature is vast. Inhibition approaches vary according to the peculiarities of the system, its metallurgy being one of the most significant. In this section we briefly review the state-of-the-art of the field of phosphonates as corrosion inhibitors, providing some characteristic examples of contributions originating from our laboratory.

Phosphonate-based corrosion inhibitors are effective in decreasing metallic corrosion in nearly neutral conditions by forming poorly soluble compounds with the metal ion existing in the solution. These metal phosphonate “complexes” precipitate onto the metallic surface to form a protective layer. Such inhibitors (often called interphase inhibitors) for cooling water treatment technology in the last decades comprise different types of phosphonic acids.¹⁷⁹ Widely used phosphonic acids are 1-hydroxyethane-1,1-diphosphonic acid (HEDP), amino-tris(methylenephosphonic acid) (AMP), hydroxyphosphonoacetic acid (HPAA), etc. Phosphonates are introduced into the system to be protected in the acid form or as alkali metal soluble salts, but readily form more stable complexes with other metal cations found in the process stream (most commonly Ca, Mg, Sr, or Ba), depending on the particular application. It should be emphasized that research in this area has been stimulated by the need to develop inhibitor formulations that are free from carcinogenic

chromates,¹⁸⁰ nitrates, nitrites, inorganic phosphorus compounds, etc. Phosphonates when blended with certain metal cations and polymers reduce the optimal inhibitor concentration needed for inhibition due to synergistic effects.¹⁸¹ Synergism is one of the important effects in the inhibition process and serves as the basis for the development of all modern corrosion inhibitor formulations.¹⁸²

In spite of the significant body of literature, evidence about the molecular identity of the thin protective metal-phosphonate films lags behind. In this section, the corrosion inhibition performance of several metal-phosphonate materials is reported and a more systematic look at their corrosion inhibition mechanisms at the molecular level is presented. These exhibit dramatically different anticorrosion efficiencies, which are linked to their molecular structure. Herein we will only mention a few examples to illustrate the point. The reader is referred to a recent review published by our group for further details.¹⁸³ These metal phosphonates are the following coordination polymers: Zn-AMP, $\{\text{Zn}(\text{AMP}) \cdot 3\text{H}_2\text{O}\}_n$; Zn-HDTMP, $\{\text{Zn}(\text{HDTMP}) \cdot \text{H}_2\text{O}\}_n$; Ca-HPAA, $\text{Ca}_3(\text{HPAA})_2(\text{H}_2\text{O})_{14}$; M (Sr, Ba)-HPAA, $\{\text{M}(\text{HPAA})(\text{H}_2\text{O})_2\}_n$.

In the following sections the corrosion rate (CR) is calculated from the equation:

$$\text{CR} = \frac{534.57 \times (\text{mass loss})}{(\text{area})(\text{time})(\text{metal density})}$$

Units: CR in mm/year, mass loss in mg, area in cm^2 , time in hours, metal density = 7.85 g cm^{-3} (for carbon steel, but this varies according to the particular metallurgy of the system).

14.8.1 Inhibitory Thin Films by the Material $\{\text{Zn}(\text{AMP}) \cdot 3\text{H}_2\text{O}\}_n$

Synergistic combinations of 1:1 molar ratio Zn^{2+} and AMP are reported to exhibit superior inhibition performance than either Zn^{2+} or AMP alone.¹⁸⁴ However, no mention is made regarding the identity of the inhibitor species involved in corrosion inhibition. Therefore, corrosion experiments were carried out in order to verify the literature results and prove that the protective material acting as a corrosion barrier is an organic-inorganic hybrid composed of Zn and AMP.¹²¹ A synergistic combination of Zn^{2+} and AMP in a 1:1 ratio (under identical conditions used to prepare crystalline Zn-AMP) offers excellent corrosion protection for carbon steel. Although differentiation between the “control” and “Zn-AMP” protected specimens is evident within the first hours, the corrosion experiment is left to proceed over a 3-day period. Based on mass loss measurements the corrosion rate for the “control” sample is 2.5 mm/year, whereas for the Zn-AMP protected sample it was 0.9 mm/year, a 270% reduction in corrosion rate. The filming material is collected and subjected to FT-IR, XRF, and EDS studies. These show that the inhibiting film is a material containing Zn (from added Zn^{2+}) and P (from added AMP) in an approximately 1:3 ratio, as expected. Fe was also present apparently originating from

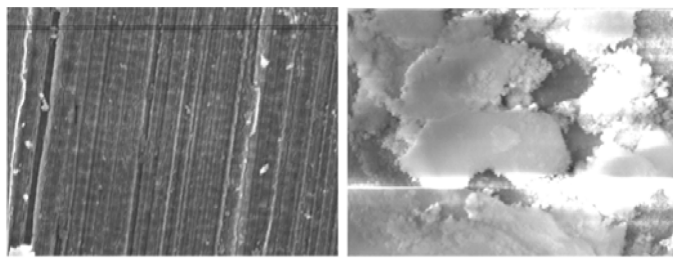


Figure 14.25 SEM images of a bare carbon steel surface (left, bar = 60 μm) and a Zn-AMP protected steel surface (right, bar = 10 μm). Deposition of an anticorrosive Zn-AMP material is obvious.

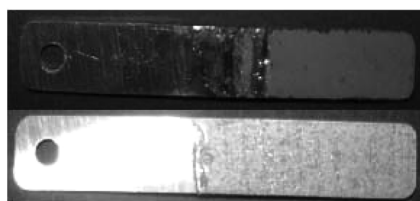


Figure 14.26 The anticorrosive effect of Zn-HDTMP films on carbon steel. The upper specimen is the “control”, no inhibitor present. Corrosion inhibition in the lower specimen by a 1 mM Zn^{2+} /HDTMP synergistic combination is obvious.

the steel specimen. FT-IR showed multiple bands associated with the phosphonate groups that closely resemble those of an authentically prepared Zn-AMP material. For comparison, EDS and XRF spectra of a “protected” and an “unprotected” region show the presence of Zn and P in the former, but complete absence in the latter. A characteristic example of a Zn-AMP film is shown in Figure 14.25 and is compared to a “bare” iron metal surface.

14.8.2 Inhibitory Thin Films by the Material $\{\text{Zn}(\text{HDTMP}) \cdot \text{H}_2\text{O}_n\}$

A combination of Zn^{2+} and HDTMP in a 1:1 ratio (under identical conditions used to prepare crystalline Zn-HDTMP) offers excellent corrosion protection for carbon steel (Figure 14.26).¹²³

Although differentiation between the “control” and “Zn-HDTMP” protected specimens is profound within the first hours, the corrosion experiment is left to proceed over a 3-day period. Based on mass loss measurements the corrosion rate for the “control” sample is 7.28 mm/year, whereas for the Zn-HDTMP protected sample 2.11 mm/year, a $\sim 170\%$ reduction in corrosion rate. The filming material is collected and subjected to FT-IR, XRF, and EDS studies.

These show that the corrosion inhibiting film is a material containing Zn^{2+} (from externally added Zn^{2+}) and P (from added HDTMP) in an approximate 1:4 ratio. Fe was also present apparently originating from the carbon steel specimen. FT-IR of the filming material showed multiple bands associated with the phosphonate groups in the 950–1200 cm^{-1} region that closely resemble those of the authentically prepared Zn-HDTMP material (Figure 14.27). For comparison, EDS and XRF spectra of a “protected” and an “unprotected” region show presence of Zn and P in the former, but complete absence in the latter.

The Zn-HDTMP material was prepared from first principles and its crystal structure was determined.¹²³ It is shown in Figure 14.28.

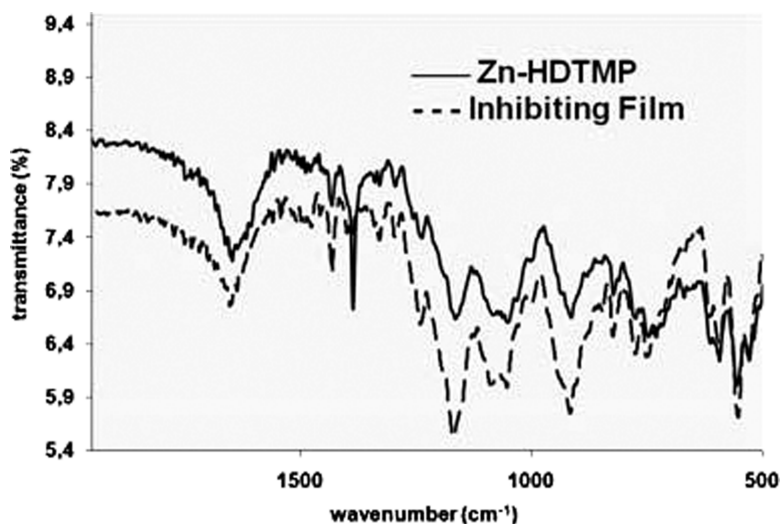


Figure 14.27 FT-IR spectra of “genuine” Zn-HDTMP and of the corrosion inhibiting film formed in situ from a 1:1 Zn^{2+} :HDTMP synergistic combination.

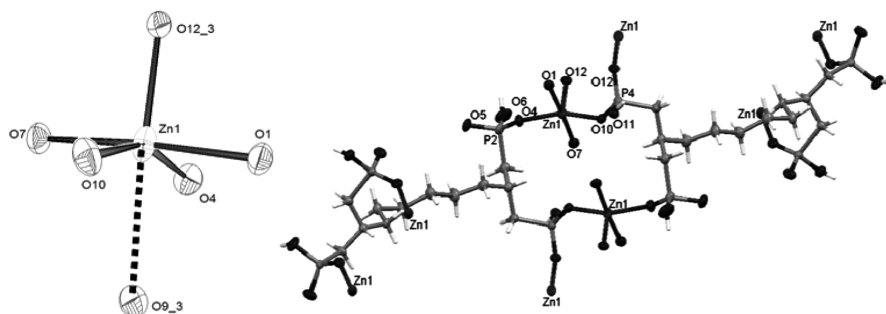


Figure 14.28 Structure of the coordination polymer $\text{Zn}(\text{HDTMP})(\text{H}_2\text{O})$: the Zn^{2+} coordination environment (left) and portion of the structure showing the extensive 18-membered ring (right). (Reproduced with permission from ref. 123.)

14.8.3 Inhibitory Thin Films by the Molecular Trimer $\text{Ca}_3(\text{HPAA})_2(\text{H}_2\text{O})_{14}$

The effectiveness of corrosion protection by synergistic combinations of Ca^{2+} and HPAA in a 1:1 ratio is dramatically pH-dependent (Figure 14.29).¹⁸⁵

At pH 2.0 mass loss from the steel specimens is profound, resulting in high corrosion rates (353×10^{-3} mm/year). However, specimen 2 (Figure 14.29) appears relatively clean from corrosion products, presumably because HPAA (either free or metal-bound) at the surface acts as a Fe-oxide dissolving agent. At pH 7.3 corrosion rates are appreciably suppressed (4×10^{-3} mm/year) in the presence of combinations of Ca^{2+} and HPAA (specimen 4), reaching nearly quantitative inhibition.

The inhibiting film is fairly uniform and contains Ca^{2+} and P (from externally added Ca^{2+} and HPAA), in an approximate 3:2 molar ratio (by EDS), suggesting a ratio of three Ca^{2+} and two HPAA^{3-} ligands. FT-IR of the filming material showed multiple bands (in the $950\text{--}1200\text{ cm}^{-1}$ region) associated with the phosphonate groups and two bands at 1590 and 1650 cm^{-1} (assigned to the $\nu_{\text{C}=\text{O}}$ stretches), that closely match those of $\text{Ca}_3(\text{HPAA})_2(\text{H}_2\text{O})_{14}$, prepared from first principles. Its molecular structure is shown in Figure 14.30. An XRD powder pattern of the Ca-HPAA anticorrosion film deposited on a carbon steel substrate is identical to that of a crystalline sample of $\text{Ca}_3(\text{HPAA})_2(\text{H}_2\text{O})_{14}$. This is unequivocal proof that the protective film on the steel surface is $\text{Ca}_3(\text{HPAA})_2(\text{H}_2\text{O})_{14}$.

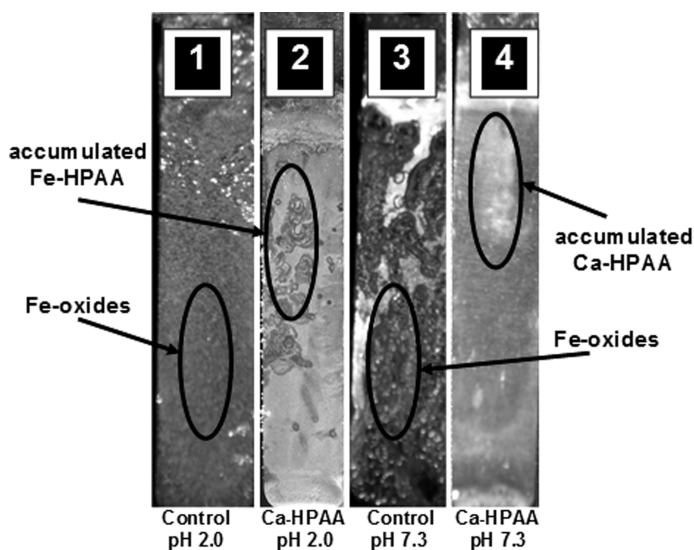


Figure 14.29 The anticorrosion protection of Ca-HPAA films on carbon steel. The effect of Ca-HPAA is especially demonstrated in specimen 4. (Reproduced with permission from ref. 185.)

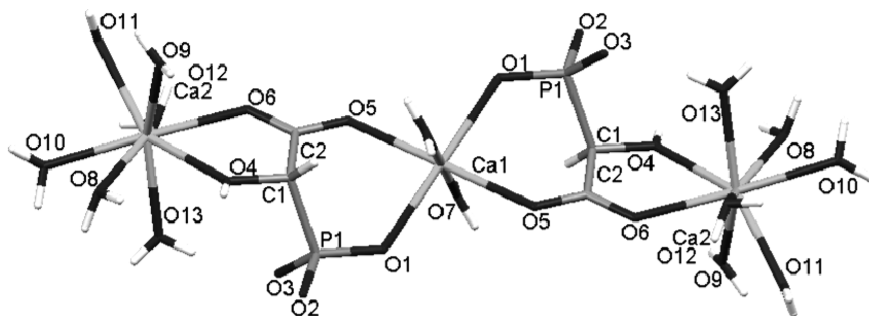


Figure 14.30 The molecular structure of the Ca-HPAA trimer. (Reproduced with permission from ref. 185.)

14.8.4 Inhibitory Thin Films by the Materials $\{M(\text{HPAA})(\text{H}_2\text{O})_2\}_n$ ($M = \text{Sr}, \text{Ba}$)

Initial experiments were focused on exposure of carbon steel specimens to synergistic combinations of M^{2+} (Sr or Ba) and HPAA in oxygenated aqueous solutions, in a 1:1 ratio (under identical conditions used to prepare crystalline M-HPAA, at pH 2.0). Although the visual effect was at first encouraging, quantification of the corrosion rates demonstrated that they were actually much higher than the “control”.^{98,99} Explanations for this lack of anti-corrosion performance at low pH regions could be that the HPAA added first reacts preferentially with the Fe-oxide layer (formed almost instantaneously upon exposure of the carbon steel surface to oxygenated water) before it interacts with soluble Sr^{2+} or Ba^{2+} . Another possibility is that Sr-HPAA or Ba-HPAA compounds that may form in solution never reach the steel surface because they undergo bulk precipitation. We have discounted this scenario, based on the following arguments. Indeed, we have observed white precipitates formed in the bulk in our corrosion experiments (pH 2.0) whose FT-IR, however, is distinctly different from those of authentically prepared Sr-HPAA or Ba-HPAA. These FT-IR spectra are the same as that of a Fe-HPAA material prepared at pH 2.0 using a Fe:HPAA ratio of 1:1, whose composition is consistent with the formula $\text{Fe}(\text{HPAA}) \cdot \text{H}_2\text{O}$. A reasonable assumption is that HPAA at the surface acts as an Fe oxide dissolving agent. We have observed a similar behavior in similar experiments with M^{2+} ($M = \text{Ca}, \text{Zn}$) and 2-phosphonobutane-1,2,4-tricarboxylic acid (PBTC).¹⁸⁶ Due to the ineffectiveness of the metal-HPAA materials to act as corrosion inhibitors at pH 2.0, no further experiments were pursued at that pH.

Hence, corrosion experiments were set up at higher pH (pH 7.3). In general, corrosion rates are lower as pH increases. This was confirmed in our “control” experiments (reduction of the corrosion rate by half). At higher pH (7.3) and in the presence of Sr^{2+} or Ba^{2+} and HPAA combinations, corrosion rates are dramatically suppressed and corrosion inhibition reaches almost 100%. Although differentiation between the “control” and “metal-HPAA”-protected specimens is profound within the first hours, the corrosion experiments were

left to proceed over a 6-day period. Anti-corrosion inhibitory activity was based on mass loss measurements. To further characterize the protective film, the corrosion specimens and film material were subjected to SEM, FT-IR, XRF, and EDS studies (Figure 14.31).

SEM images reveal a fairly uniform inhibiting film. This coating was found (by EDS, Figure 14.31, right) to contain M^{2+} (Sr or Ba from externally added salts) and P (from added HPAAs), in an approximate 1:1 molar ratio. Fe was also present, apparently originating from the carbon steel specimen.

Furthermore, a complementary study of the inhibiting film was pursued by FT-IR spectroscopy. Figure 14.32 shows comparative FT-IR spectra of the

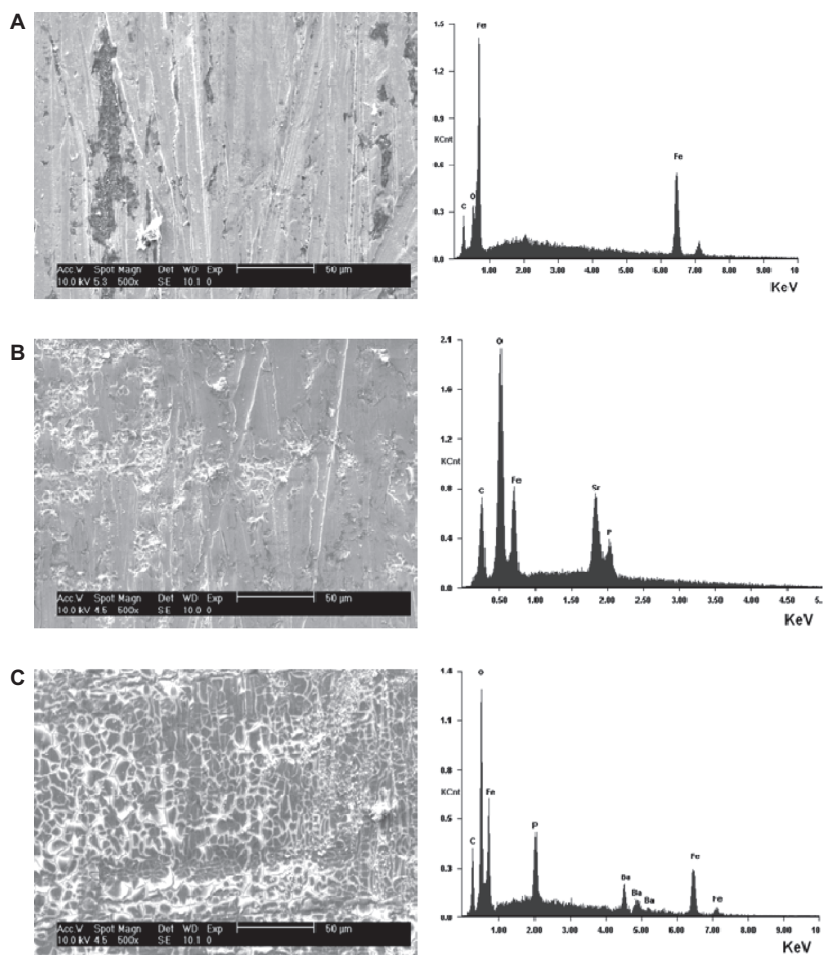


Figure 14.31 Morphology of corroded and metal-HPAA-protected steel surfaces by SEM: control (A), Sr-HPAA (B), and Ba-HPAA (C) at pH 7.3. Occasional film cracking is due to drying. Identification of film components (Fe, C, O, Sr, Ba, and P) was possible by EDS: control (A), Sr-HPAA (B), and Ba-HPAA (C). (Reproduced with permission from ref. 99.)

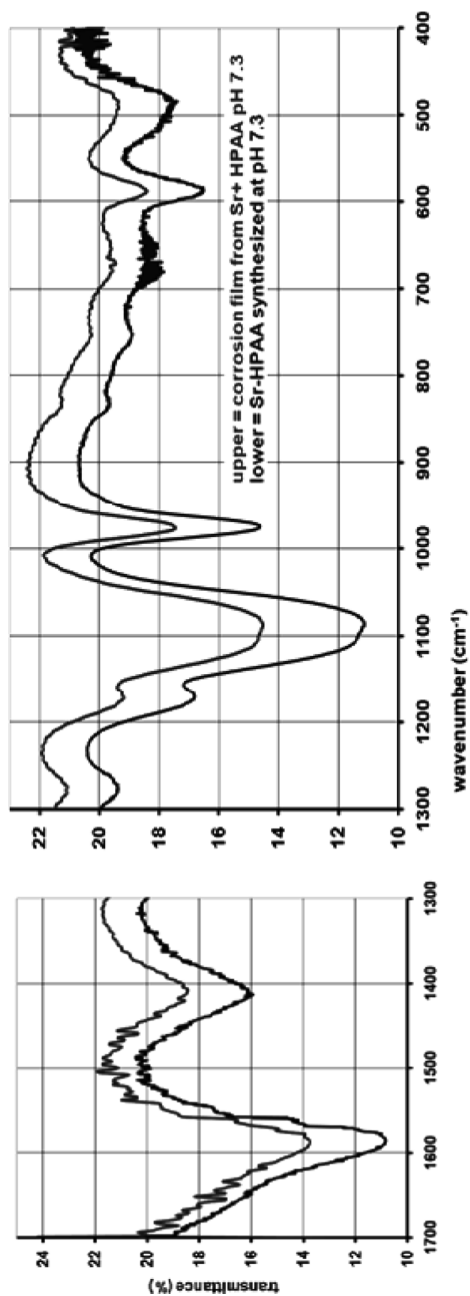


Figure 14.32 FT-IR of the anti-corrosion protective film formed by combination of Sr²⁺ and HPAA at pH 7.3 and, for comparison, of Sr-HPAA synthesized at pH 7.3. Left: $\nu(\text{C}=\text{O})$ asymmetric and symmetric stretching vibrations. Right: vibrations associated with the phosphonate group. (Reproduced with permission from ref. 99.)

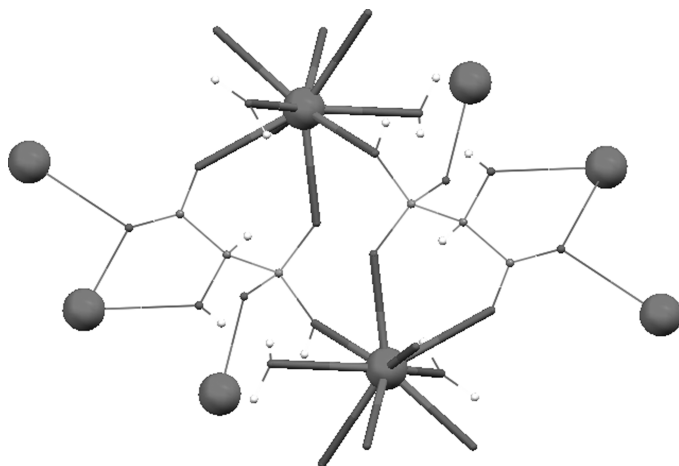


Figure 14.33 Coordination function of the HPAA ligand in $M[(\text{HPAA})(\text{H}_2\text{O})_3] \cdot \text{H}_2\text{O}$, with metal ions as exaggerated spheres.

filming material (from a corrosion experiment with Sr^{2+} and HPAA at pH 7.3) and a Sr-HPAA material that was synthesized at pH 7.3. A similar FT-IR spectrum was obtained for the Ba^{2+} /HPAA system. It is obvious that there is an excellent agreement between the two spectra.

The materials $\{M(\text{HPAA})(\text{H}_2\text{O})_2\}_n$ ($M = \text{Sr}, \text{Ba}$) are isostructural, and their structure is depicted in Figure 14.33.

The anti-corrosion coatings composed of Sr-HPAA or Ba-HPAA function as corrosion inhibitors by reducing the cathodic current. This results in lower corrosion rates. The films prevent oxygen diffusion towards the steel surface. This phenomenon is well-known for phosphonate additives.¹⁸⁷

14.8.5 Inhibitory Thin Films by other Structurally Characterized Metal Phosphonate Materials

Similar studies such as that mentioned above have been carried out. These included the metal phosphonates $\{\text{Ca}(\text{PBTC})(\text{H}_2\text{O})_2 \cdot 2\text{H}_2\text{O}\}_n$,¹⁸⁶ $\{M(\text{PMIDA})\}_n$ ($M = \text{Ca}, \text{Sr}, \text{Ba}$),¹⁷² $\{M[(\text{EDTMP})(\text{H}_2\text{O})_2] \cdot \text{H}_2\text{O}\}_n$ ($M = \text{Ca}, \text{Sr}$),¹⁸⁸ and $\{\text{Ba}[(\text{HDTMP})(\text{H}_2\text{O})_6] \cdot 2\text{H}_2\text{O}\}_n$.¹⁸⁹ The reader is referred to the above original papers for further details.

14.8.6 A “Holistic” Look at Metal Phosphonate Materials as Corrosion Inhibitors

Metallic corrosion is a phenomenon affected by several factors. It is well established that pH is one of the major factors affecting corrosion rates.

The more acidic the fluid (water) in contact with the metal surface, the more aggressive the corrosion. Therefore, pH plays a profound role in corrosion inhibition as well. In Figure 14.34, the performance of several metal phosphonate corrosion inhibitors has been systematically gathered and plotted. There are a number of important observations to be discussed. At higher pH regions (~ 7) most metal phosphonate coatings perform well. At low pH regions (< 3) corrosion inhibition is more challenging. This may have to do with incomplete formation of the protective coating. In addition, the high concentration of H^+ and the resulting high corrosion rates may be prevailing over the formation of the metal phosphonate protective coating.

The results with Ca-PBTC and Zn-PBTC require further discussion. Corrosion rates in the presence of inhibitor are *higher* than those for the control (no inhibitor). This, at a first glance, is contrary to results obtained with several other inhibitors. This may be explained by several arguments. First, the metal-phosphonate film may not be robust, but porous in its microscopic nature. This, as mentioned before, would lead to localized attack and metal pitting. Such phenomena have not been observed upon examination of the metal specimens after the corrosion experiments. Second, the metal phosphonate (Ca, or Zn-PBTC) is too soluble to deposit onto the metal surface, so it does not form a protective and anticorrosion thin film. This argument would be consistent with literature data on metal-PBTC complex formation constants (4.4 for Ca-PBTC and 8.3 for Zn-PBTC) that are considered to be very low.⁶⁴ The difference in complex formation constants between Ca- and Zn-PBTC would be consistent with the fact that Zn-PBTC is a more effective corrosion inhibitor than Ca-PBTC, as long as both inhibitors form films (albeit unstable) on the metal surface. If film formation does not take place, then corrosion rates in the presence of Ca-PBTC or Zn-PBTC would be the same as the control, which is not the case. Therefore, the results obtained with Ca-PBTC and Zn-PBTC, indicate that these materials are soluble and due to their acidic nature they actually act as metal dissolvers rather than corrosion inhibitors.

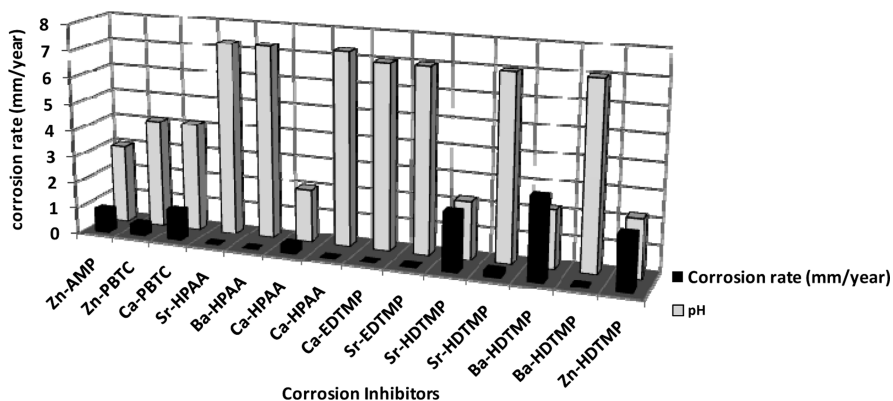


Figure 14.34 Corrosion rates of metal phosphonate-protected surfaces as a function of pH.

The Zn-HDTMP material by virtue of its long chain linker between the two amino-bis(methylenephosphonate) moieties might be thought of as a porous material. However, porosity measurements on this and the other phosphonates show absence of any porous structure. Therefore, differences in porosity cannot be invoked to explain the various anticorrosion properties of these metal-phosphonate materials.

Lastly, the ability of a metal-phosphonate corrosion inhibitor to adhere onto the metal surface plays a vital role in corrosion efficacy. Bulk precipitation of a metal-phosphonate complex will lead to loss of active inhibitor to precipitation, leading to insufficient levels for thin-film formation. Surface adherence of the inhibitor films is a property that cannot be precisely predicted. However, it is a necessary condition for acceptable inhibition. In addition, the metal-phosphonate protective layer has to be robust and uniform.

Corrosion is a vast scientific field; however, it presents several facets that touch upon economics and people.¹⁹⁰ For example, the overall demand for corrosion inhibitors after a rather constant rise of $\sim 4.4\%$ /year, reached \$ 1.6 billion in 2006 in the USA.¹⁹¹ The petroleum refining sector was expected to have a \sim \$ 400 million share in this. Corrosion is an economical burden for several industry sectors. Research on the subject has been active for several decades.^{192,193} The solution to this complicated issue requires a multi-disciplinary approach that unifies researchers from a diverse list of scientific and technological disciplines: chemistry, chemical engineering, electrochemistry, materials science, engineering, and many others.

In this section, our contribution to advancing solutions for corrosion issues relevant to industrial problems lies with the study of the corrosion event and its inhibition *at the molecular level*. In this context, we have shown that conveniently synthesized and structurally characterized organic-inorganic hybrid polymeric materials can act as protective corrosion inhibitors.

An ideal phosphonate corrosion inhibitor of the “complexing type” is required to possess the following features:

- (a) it must be capable of generating metal-phosphonate thin films on the surface to be protected
- (b) it should not form very soluble metal complexes, because these will not eventually “deposit” onto the metal surface, but will remain soluble in the bulk
- (c) it should not form sparingly soluble metal complexes because these may never reach the metal surface to achieve inhibition, but may generate undesirable deposits in the bulk or on other critical system surfaces
- (d) its metal complexes generated by controlled deposition on the metal surface must create dense thin films with robust structure. If the anticorrosion film is non-uniform or porous, then uneven oxygen permeation may create sites for localized attack, leading to pitting of the metal surface.

14.9 Gas Storage

Hybrid organic–inorganic microporous materials, particularly metal carboxylate frameworks, are of great importance in solid-state and materials chemistry. Many microporous, thermally stable to 700 K, 3D connected framework structures have been discovered that have pores up to ca. 20 Å in free diameter, and have remarkable adsorption properties, including very high surface areas, structural flexibility, and uncoordinated metal adsorption sites. MOF-5,¹⁹⁴ MIL-100,¹⁹⁵ and HKUST-1¹⁹⁶ are among the widely known carboxylate MOFs. Other families of porous MOFs including those based on amines, such as zeolitic imidazoles,¹⁹⁷ mixed amine-carboxylates,¹⁹⁸ and amino acids¹⁹⁹ have also attracted attention.

Metal phosphonates were among the first microporous organic–inorganic hybrid adsorbents to be investigated. They offer an alternative set of chemical and structural possibilities but none of them is being possessed of pores larger than 6 Å resulting to low uptake of adsorbates. In metal phosphonate chemistry there is a rich variety of phosphonate building units that can be used as reagents and form strong bonds with a range of metal cations when they bind through one, two, or three oxygen atoms per phosphonate groups. Due to the fact that the O₃P–C bond is stable to elevated temperatures, there is a great prospect for the preparation of thermally stable phosphonate frameworks that would be competitive with metal carboxylate MOFs in applications.

Efforts for the synthesis of structures with larger pores and adsorption capacities using *N,N'*-piperazinebis(methylenephosphonic acid) (H₄L) were successfully accomplished, resulting in the first large pore metal phosphonates which followed up the syntheses of divalent metal piperazinebis(methylenephosphonate)s of Co(II), Mn(II), Fe(II), and Ni(II) among which the nickel and cobalt bis(phosphonate)s showed remarkable pore volume and thermal stability.²⁰⁰

Additional reactions of Fe(II), Co(II), Ni(II) acetates with H₄L at pH values below 6.5, resulted in the formation of structure type [Mn(H₂O)₂ L] · 5.4 H₂O materials. Their framework is based on inorganic columns of helical chains of edge-sharing NiO₅N octahedra and comprises the first porous solids in which the ligand coordinates through both oxygen and nitrogen atoms. The arrangement of inorganic chains and organic linkers leaves a structure with a hexagonal array of channels with a free diameter taking into account van der Waals radii of hydrogen atoms, of ca. 10 Å. Decomposition of materials occurs above 400 °C leading to the conversion of unit cell from rhombohedral to primitive triclinic for cobalt and nickel versions. Using the 2-methylpiperazine version of the bis-phosphonic acid in the syntheses gives the same structure materials for nickel and cobalt versions. After dehydration of Ni₂L' the symmetry remains rhombohedral resulting to higher absorption of nitrogen in regard to Ni₂L.

Using cobalt acetate in reactions with H₄L' gives a novel structural material where the inorganic unit is composed of chains of tetramers of octahedral cobalt cations linked by three phosphonate units. Coordination of outer cobalt

anions by three phosphonate oxygens, nitrogen of the piperazine ring, and two remaining oxygens from acetate groups and water molecules sets up inorganic columns which are linked to three other identical columns of piperazine units in chair conformation. Upon dehydration the structure remains crystalline, without change in symmetry and indicates channels with free dimension of around 7 Å, showing unremarkable nitrogen adsorption. Both phosphonate structures offer potential as adsorbents. Due to the fact that they can be prepared with a racemic mixture of *N,N'*-2-methylpiperazinebis(phosphonic acid)s there are great possibilities for chiral separations, while the use of the 2-methylpiperazine derivative of the acid is both preventing distortion of structures upon dehydration and increasing nitrogen absorption. Moreover, accessible metal sites show Lewis acidity resulting in the catalytic activity of materials as well as the nature of inorganic chains in these solids suggest their interesting magnetic properties.

Recently, porous divalent metal phosphonates have been prepared comprising Fe, Co, and Ni, materials labeled as STA-12, being the first fully crystalline phosphonate MOFs with pores approaching 1 nm and specific pore volume approaching values observed for large pore zeolites.²⁰¹ The nickel version of STA-12 is highly porous containing channels filled with physisorbed and chemisorbed water molecules coordinated to the nickel cations when fully hydrated. The framework of the as-prepared solid is built from helical chains of edge-sharing NiO₅N octahedra, linked into a honeycomb arrangement via the ligands. The ligand coordinates to the metal atoms of the inorganic chain via phosphonate oxygen atoms and the piperazine ring N atom, a structural feature which imparts thermal stability up to 650 K. The structure of Ni-STA-12 at different levels of hydration reveals changes in the local structure of the framework during reversible dehydration and rehydration. H₂ and CO are excellent probes of adsorption sites at low temperatures, while CO₂, CH₃OH, CD₃CN, and CH₄ are useful probes at room temperature in terms of the fully dehydrated sample. All measurements were carried out at 303 K in order to evaluate the adsorption properties of the material for potential storage and separation applications. These greenhouse gases have been chosen both with respect to their relevance in several applications and also to permit a comparison between interactions of the adsorbent with molecules possessing a significant quadrupole moment (CO₂) and without any permanent moment (CH₄). During reversible dehydration, significant structural rearrangement arises with a symmetry change from rhombohedral to triclinic resulting in a small reduction in pore size. Rehydration has been found to be rapid, whereas dehydration takes place in two main steps including the loss of physisorbed water after gentle heating to give a rhombohedral structure while chemisorbed water is lost completely above 373 K to give a triclinic unit cell. The fully dehydrated structure displays remarkable structural complexity including NiO₄N coordination polyhedra intermediate between tetragonal pyramids and trigonal bipyramids, linked via either edge- or corner-sharing. The structure has adapted to water loss by movement of the phosphonate tetrahedra and transformation of the nickel coordination to NiO₄N polyhedral, resulting in the

formation of a number of adsorption sites that are different from those observed in other MOFs or zeolites and include coordinatively unsaturated nickel sites and accessible P=O groups on one in three phosphonates as well as sites on the organic linkers. Interactions of these sites with adsorbed probe molecules confirm the presence of Lewis acid sites of moderate strength. In the partially dehydrated form, free and hydrogen bonded hydroxyl groups are present instead. Both types of samples exhibit permanent porosity in the adsorption of gases but higher heats and capacity are observed in the fully dehydrated solid. Additional adsorption data of H₂ and CO at 77 K show strong adsorption of the former, and strong interactions for the latter suggesting that the structure can adjust to accommodate the CO at all nickel sites but in terms of H₂ only on the accessible nickel cation sites. The different types of nickel cations act as Lewis acid sites with different strengths of interaction, depending on their local geometry, and there is also evidence that that P=O groups interact weakly. This unusual array of adsorption sites is expected to show unusual adsorption selectivity for separation and purification whereas the structure can show characteristic catalytic activities.

A tetrahedral phosphonate ligand 1,3,5,7-tetrakis(4-phosphonatophenyl)adamantane (LH₈) was designed to prevent the formation of simple layers and direct the formation of an open framework upon metal complexation.²⁰² The tetrahedral ligand forms large diamondoid motifs rather than densely packed arrangement complexes with Ti⁴⁺ and V³⁺, which show nitrogen sorption, as well as the crystal structure of diamondoid solid [Cu₃(H₃L)(OH)(H₂O)₃]·H₂O·MeOH which displays permanent porosity as confirmed by CO₂ sorption analysis. All diamondoid nets have a topology which readily enables interpenetration to fill potential void space but despite this, an open channel structure is still formed. The clusters are formed by an “anti-SBU” approach and the geometry of L is structure determining as it directs the topology and geometry of the resultant metal cluster. Magnetic measurements on [Cu₃(H₃L)(OH)(H₂O)₃]·H₂O·MeOH indicate that antiferromagnetic exchange interactions occur between the copper centers within the clusters.

Layered salts of zirconium phosphate (ZrP) yields pillared scaffolds where the surface phosphate groups in γ -ZrP layers can be replaced by phosphonates and hypophosphite which leads to drastic changes in the porosity. The incorporation of rigid 4,4'-terpenyldiphosphonate into γ -ZrP followed by further exchange of residual surface phosphate groups with hypophosphite gives a much more porous, non-polar solid.²⁰³ The exchange reaction with 4,4'-terpenyldiphosphonate leads to material **I** where some of the diphosphonates do not form pillars but are bonded only by one end to the organic layers. Treatment of this material with hypophosphorous acid gives a product with similar hydrogen and carbon content (material **II**) which does not involve loss of terpenyldiphosphonate but shows reduction in crystallinity and interlayer distance. Hypophosphite is not incorporated into the matrix contrary to phosphate and phosphonate groups. The reaction is not topotactic, as occurs in the case of pillared γ -ZrP with polyethylenoxadiphosphonates, but in turn directs the formation of a mixed phase leading to the production of a much

more porous solid which takes up hydrogen in amounts of $74 \text{ cm}^3 \text{ g}^{-1}$ at 650 Torr.

Pillared clays are a new class of microporous solids prepared from the intercalation of polyoxocations in the interlayer region of layered aluminosilicates, possessing microporosity. As this fact is not restricted to aluminosilicates, many other porous pillared materials can be designed, showing initial interest in structures of different layered metal phosphonates, arsenates, and phosphates, derived from various combinations of tetrahedral and octahedral building blocks. Up to this point three main layered structures are known: α -layered structure, γ -layered structure, and layered compounds of general formula $\text{ZrPO}_4\text{LL}'$.²⁰⁴ All layered structures can be pillared both with organic and inorganic pillars to obtain microporous and mesoporous compounds. Moreover, some engineered zirconium diphosphonate compounds in which special pillars are employed result in materials with particular characteristics such as topochemical reactivity, electron transfer, and nonlinear optical properties whereas photochromism, via the photoreduction of pillars containing viologen is promising in solar energy storage application.

As it concerns α -layered structure, the zirconium bis(monohydrogenphosphate) monohydrated (hereafter α -ZrP) is the most representative member. In this compound the metal shares six oxygens with six different $\text{O}_3\text{P-OH}$ groups where a monolayer of metal atoms, bridged by monohydrogenphosphate groups lying alternately above and below it, share three of their oxygens with the tetravalent metal. The forces holding the layers together are of van der Waals type and the intercalated water molecules form hydrogen bonding with the P-OH groups belonging to only one side of the layers. In the γ -layered structure the zirconium atoms lie in two different planes and are bonded by tetrahedral PO_4 and H_2PO_4 groups. The PO_4 group shares all four oxygens with zirconium atoms while the H_2PO_4 shares two oxygens with two different zirconium atoms. Adjacent layers are linked by hydrogen bonds involving the water molecules and the $-\text{P}(\text{OH})_2$ groups. The compounds of this class can be formulated as $\text{ZrPO}_4\text{LL}'$ in which L is a neutral ligand and L' is an anionic monovalent ligand (see Chapter 1).

Although α - and γ -layers have the same chemical composition, their structural characteristics are quite different, such as distances between active sites, thickness and flexibility of the layers, and interlayer hydrogen bonds, affecting the mechanism of intercalation, the exfoliation, and the distribution of the intercalated species in the interlayer region which impacts the porosity in the interlayer of layered materials. The driving force for the intercalation of pillars, or their precursors, is their interaction with some active sites present on the surface of the lamellae which have polar character. The reciprocal value which corresponds to the surface density of the active sites on one side of a layer is usually called *free area*. As it concerns α -ZrP, the active sites are the acid $-\text{OH}$ groups covalently bonded to phosphorus whereas in the case of γ -ZrP there are two acid $-\text{OH}$ groups bonded to the same phosphorus but only one is active for intercalation of large pillars. The effect of distance between active sites is established by the interaction of a divalent pillar with two active sites belonging

to adjacent layers inducing a lateral distance which corresponds to the distance between the two active sites. If the latter distance is too short, the pillars tend to be overcrowded in the interlayer region and no microporosity can be obtained unless special precautions are taken. Moreover, the tendency towards formation of solid solutions in the interlayer region is higher in solids with rigid layers. In the case of pillaring with polyoxocations, the more rigid the layers are the greater the possibility of the formation of stable solid solutions in which the polyoxocations are laterally spaced by small intercalated species that can then be removed to obtain or to increase the microporosity in the interlayer region. In some layer compounds interlayer hydrogen bonds are present, a fact that has to be taken into consideration when pillaring with large molecular species must be obtained from colloidal dispersion of the exfoliated layered compound. As it concerns layered metal phosphates, γ -ZrP exhibits the greater thickness and the greater layer rigidity; as a result it exhibits the greater tendency to the formation of solid solutions.

If in the synthesis of α -ZrP, phosphoric acid is replaced by either phenylphosphonic or diphosphonic acid, then the zirconium phosphonate or diphosphonate which results respectively has the same inorganic network as α -ZrP. A meaningful difference, however, is that in the case of phenylphosphonic acid the monovalent organic radicals pendant in the interlayer region whereas in diphosphonates, inorganic layers are covalently joined by divalent ones. A significant finding for these materials is that the surface area of those that possess a low degree of crystallinity is largely due to intercrystal mesoporosity, a fact related to the high flexibility of the α -layers. The problem is mitigated by the use of pillars with cross sections larger than 0.24 nm^2 . One of these pillars, 3,3',5,5'-tetramethylbiphenyldiphosphonic acid, was prepared exhibiting a high phosphate percentage, a good degree of crystallinity, and interlayer microporosity. Additionally, large excess of phosphorous acid in the synthesis of zirconium phosphate-diphosphonates induces the formation of a high percentage of mesopores with high specific surface area and possibility of modification of the diameter of the mesopores by changing the ratio and concentrations of the reagents. Organic pillared compounds of γ -ZrP, unlike those of α -ZrP, that can be prepared only by direct synthesis, have been obtained only by topotactic replacement of $\text{O}_2\text{P}(\text{OH})_2^-$ lying in the external sides of the γ -lamellae with $\text{O}_2(\text{OH})\text{P-R-P}(\text{OH})\text{O}_2^-$ group. Reaction takes place with both monophosphonic and diphosphonic acids and is homologous to the replacement of monohydrogen phosphate with phosphonate groups in α -ZrP. However, the topotactic replacement of the monohydrogen phosphate groups with phosphonate groups in α -ZrP can take place only on the surface of the microcrystals, while in γ -ZrP the replacement occurs in the interlayer region. A variety of organic derivatives has been obtained using aliphatic and aromatic phosphinic and phosphonic acids, X-ray diffraction patterns of which prove that the γ -layer framework remains unaltered as well as that the interlayer groups influence the interlayer distance. Accommodation of the organic moieties in the interlayer region by means of simple structural models derived on the basis of the structure of the original γ -ZrP indicate that a and b dimensions

are sufficiently large to accommodate one linear alkyl chain per each zirconium and as a result full conversion can be expected for n-alkylphosphonic acid. Though, a different situation is found for phenylphosphonic acid as the rigidity of the aromatic ring causes a steric hindrance with the adjacent -OH groups. In the case of phenylphosphonic group, the steric hindrance due to hydrogen atoms is markedly smaller and 100% of replacement is observed whereas partial replacement is perceived when using dimethylphosphonic acid. All these derivatives can find practical application as catalysts or solid electrolytes and especially the compound containing benzenesulfonic acid groups that exhibit a very high protonic conduction.

When diphosphonic acid with alkyl chains is used for topotactic reaction with exfoliated γ -ZrP, compounds of composition $\text{ZrPO}_4(\text{H}_2\text{PO}_4)_{1-x}(\text{HO}_3\text{P}(\text{CH}_2)_m\text{-PO}_3\text{H})_{x/2} \cdot n\text{H}_2\text{O}$ result, in which the alkyl chains act as pillars. The pillaring does not occur by non-rigid R organic radicals and is of significant interest because of the variation of the conformation of the pillars. Pillared compounds with $m = 4, 6, 10, 12$ are revealed that the interlayer distance of hydrate samples depend linearly on the m value. For anhydrous samples, the linear dependence of the interlayer distance from m is found at very high pillaring percentages while is almost independent for low pillaring percentages. The effect of alteration of elongation and shortening of the interlayer distance is called *accordion effect* and is reversible.²⁰⁵ The compounds at low pillaring percentages act as layer solids with chained adjacent layers. If the lateral distance is large enough to permit collapse of the chains the interlayer distance depends on the species intercalated. However, the maximum interlayer distance of chained layer solids is fixed by the length of the alkyl chain joining the layers. As a result these pillared solids behave as intermediates between layer solids and pillared compounds with rigid pillars. Due to the fact that solid solutions are formed at low pillaring percentages and very long alkyl chains can be used as non-rigid pillars, interlayer spaces as large as $2 \times 2 \times 3$ units are possible. Such interlayer spaces can be pertained as molecular vessels in which selective reactions can be carried out.

The incorporation of rigid 4,4'-biphenyldiphosphonic (BPDP) and phosphorous acids (in different ratios) into aluminum salts results in amorphous microporous materials designated as UAM-150, UAM-151, and UAM-152.²⁰⁶ H_2 adsorption data reveal its augmentation as the amount of phosphorous acid increases whereas the H_2 intake displayed by material UAM-152 is close to the highest reported for organic-inorganic materials at 77 K and atmospheric pressure. Moreover, the last two materials show lower C % contents and inferior TGA losses at high temperature, which strongly support that phosphorous acid incorporates into the matrix. Further measurements indicate adsorption in wide micropores and on external surface and prove that the incorporation of H_3PO_4 to the crystals led to a substantial increase in porosity. Pore size distribution analysis for material UAM-150 shows mainly micropores and ultra micropores and only the latter for material UAM-152, a fact that intimates strong interactions between H_2 and the material due to increased van der Waals contact areas associated with very small pore sizes. Finally the fact

that UAM-152 adsorbed 1.64% H₂ shows a relatively limited surface area although most of the molecular systems adsorbing this amount of H₂ or even lower have areas even well above this value. The authors stated that a large specific surface area is not a prerequisite in design of porous materials for efficient hydrogen storage.

14.10 Ion Absorption

Bein *et al.* have recently published a significant paper on the exceptional ion-exchange selectivity of a flexible open-framework sodium-lanthanum(III) tetrakis-phosphonate, NaLa[(HO₃P)₂CH-C₆H₄-CH(PO₃H)₂]₂·4H₂O.²⁰⁷ The exchange of the Na⁺ ions in this material with alkaline earth, alkaline, and selected transition metal ions was studied. In aqueous media, the Na⁺ ions hosted in the channels of the structure can be exchanged with other monovalent ions with ionic radii ranging from 0.76 Å (Li⁺) to 1.52 Å (Rb⁺), while divalent ions in the same size range are rejected.

Two open framework and microporous materials, [Pb₇(HEDT-P)₂(H₂O)]·7H₂O and [Zn₂(H₄EDTP)]·2H₂O [H₈EDTP = *N,N,N',N'*-ethylenediamine-tetrakis(methylenephosphonic acid)], have been synthesized and structurally characterized.²⁰⁸ Both materials adsorbed >96% of Fe³⁺ in aqueous solutions. They were also found to adsorb Fe³⁺ ions selectively over other metal ions, such as Ca²⁺, Cr²⁺, Mn²⁺, Cu²⁺, Zn²⁺, Cd²⁺.

Another (non-phosphonate) coordination polymer material, [Ba₂(L)(H₂O)₅]Cl, where L is the trianion of 1,3,5-tris(sulfomethyl)benzene, was found to exchange the chloride ions of the structure for fluoride ions in a facile manner (80% yield).²⁰⁹ This exchange was quantified by elemental analyses, gravimetric determination, and ¹⁹F NMR spectroscopy. Confirmation of retention of structure is provided by standardized powder X-ray diffraction experiments. This last point is notable as the F⁻ analog of the structure is not attainable by a direct synthesis.

Several new tin(IV) nitrilotris(methylene)triphosphonates of different composition have been synthesized by a gel method in granular form (as spherical beads).²¹⁰ The ion exchange behavior of tin(IV) nitrilotris(methylene)triphosphonates towards alkali, alkaline earth, and some transition metal ions in individual and complex solutions were studied. It was found that these exchangers contain highly acidic adsorption sites, which enables them to operate efficiently even at pH close to 0. High affinity of the tin(IV) nitrilotris(methylene)triphosphonates for lead, cadmium, and copper in acid solutions makes them promising for treatment of some technological solutions and waste.

A novel hybrid ion-exchange material, zirconium-hydroxy ethylidene diphosphonate [ZrHEDP], has been synthesized by the sol-gel technique.²¹¹ No crystal structure is available for this material. ZrHEDP was investigated for its possible use as an ion exchanger. The Na⁺ ion-exchange capacity of the material was determined, and kinetics and thermodynamics of exchange for the

metal ions Cu^{II} , Ni^{II} , Zn^{II} , and Mn^{II} towards ZrHEDP were studied. The sorption of the metal ions followed the order $\text{Zn}^{\text{II}} > \text{Cu}^{\text{II}} > \text{Mn}^{\text{II}} \approx \text{Ni}^{\text{II}}$.

Mesoporous surface-phosphonated titania, hierarchically meso-/macroporous titania phosphonate, and titanium phosphonate hybrid adsorbents have been prepared by a simple template-free nanoparticle-assembly procedure with the use of different kinds of organophosphonic acids as the coupling molecules.^{212,213} The phosphonates used were 1-hydroxy ethylidene-1,1-diphosphonic acid (HEDP), ethylenediamine-tetra(methylene phosphonic acid) (EDTMP), and diethylenetriamine-penta(methylene phosphonic acid) (DTPMP). With the increase of the molar ratio of the original added phosphonic acid and tetrabutyl titanate, the structural phase transformed from crystalline phosphonated titania to semicrystalline titania-phosphonated hybrid to amorphous titanium phosphonate, and simultaneously the nanoarchitecture also changed from disordered mesoporous to hierarchically meso-/macroporous structure. The selective complexation affinity with different metal ions on different hybrid adsorbents depends on the nature and positions of organic functional groups in the synthesized samples. Mesoporous organophosphonated titanias exhibited unique selective complexation affinity for Cd^{2+} with the sequence of $\text{Pb}^{2+} < \text{Cu}^{2+} < \text{Cd}^{2+}$, and titania phosphonate showed a selective complexation affinity for Cu^{2+} with the sequence of $\text{Cd}^{2+} < \text{Pb}^{2+} < \text{Cu}^{2+}$, while hierarchical meso-/macroporous titanium phosphonates with intra-framework ethylenediamine groups exhibited a large capacity for all the three kinds of ion adsorption with a preference sequence of $\text{Cd}^{2+} < \text{Cu}^{2+} < \text{Pb}^{2+}$ and effective regeneration ability. Also, a β -cyclodextrin-added derivative of macroporous titanium organophosphonate was prepared.²¹⁴ The obtained macroporous titanium phosphonate materials exhibited selective absorption of Cu^{2+} ions compared to Cd^{2+} and Pb^{2+} .

Phosphonic acids have also been immobilized (grafted) onto polymeric matrices. Although these materials are not “technically” metal phosphonates, a brief reference to some of these may be useful to the reader. These polymeric resins have been used successfully for the removal of metal ions from aqueous solutions. Popa *et al.* reported the preparation and characterization of some chelating resins, phosphonate grafted on polystyrene-divinylbenzene supports.²¹⁵ The resins were prepared by an Arbuzov-type reaction between chloromethyl polystyrene-divinylbenzene copolymers and triethylphosphite, yielding the phosphonate ester copolymer (resin A). This can be hydrolyzed by HCl to yield the phosphonate/phosphonic acid copolymer (resin B). The total sorption capacity of the phosphonate ester-functionalized resin (A) and phosphonate/phosphonic acid-functionalized resin (B) for divalent metal ions such as Ca^{2+} , Cu^{2+} , and Ni^{2+} was studied in aqueous solutions. Resin A retains ~ 3.25 mg Ca^{2+} /g copolymer, 2.75 mg Cu^{2+} /g copolymer, but retains no Ni^{2+} at pH = 1. On the other hand, resin B retains 8.46 mg Ca^{2+} /g copolymer, 7.17 mg Cu^{2+} /g copolymer, and no Ni^{2+} at pH = 1. Efficient Ni^{2+} retention was observed at pH = 7 only for the phosphonate/phosphonic acid-functionalized resin (B) at the level of 19 mg Ni^{2+} /g polymer B. Polymer A was incapable of retaining Ni^{2+} at pH = 7.

Separation of hafnium and zirconium was achieved by applying resins with $-\text{PO}_3\text{H}_2$ groups and defined structure.²¹⁶ Diphonix[®] resin is a commercially available chelating cation exchanger containing diphosphonic, sulfonic, and carboxylic acid groups bonded to the polymer matrix. The best medium for separation of hafnium and zirconium was 0.5 M sulfuric acid. Decrease in temperature from 22 °C to 5 °C lowered the degree of metal separation, while lower flow rates through the column increased separation ability. Under the best examined conditions, a 10-fold decrease of initial content of hafnium in zirconium could be achieved, with a 45 % efficiency of zirconium recovery. These results prove that Diphonix[®] resin is very promising for the separation of zirconium from hafnium.

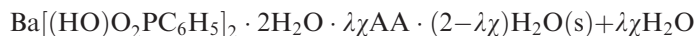
14.11 Intercalation

The earliest reported data on the intercalation chemistry described the insertion of sulfuric acid into lamellar graphite in 1841. The field of intercalation chemistry expanded dramatically over the last four decades, as more and more new inorganic layered materials were discovered as potential “hosts” to “guest” molecules. As with several other scientific fields, potential applications were the drivers of intercalation development: adsorption, ion exchange, catalysis, proton and ion conductivity, etc. Host materials have to possess high thermal stability, resistance to chemical oxidation, and selectivity to ions and molecules. Most importantly, they must be able to expand their interlamellar space when guest molecules are to be inserted.^{217,218}

Layered metal phosphonates have been extensively used for intercalation applications (for reviews, see references 219 and 220). Most lamellar metal mono-phosphonate compounds have the general formula $\text{M}(\text{O}_3\text{PR})_x \cdot n\text{H}_2\text{O}$, for various metals (M), where R is an aliphatic or aromatic group. Molecules such as *n*-alkylmonoamines,^{221–224} *n*-alkyldiamines,²²⁵ aromatic amines (pyridine and the likes),²²⁶ dendritic polyamines,²²⁷ etc.

Ruiz and Airoidi have reported on the interaction of *n*-alkylmonoamines, $\text{R}-(\text{CH}_2)_n-\text{NH}_2$ ($n=0-6$) with zirconium phenylphosphonate solid, $\text{Zr}(\text{O}_3\text{PC}_6\text{H}_5)_2$.²²⁸ It may be expected that in neat amine (very high pH), a replacement of the phosphonate by OH^- likely takes place. Thus, a subsequent metal–N interaction may be possible leading to the amine taken up by the solid. In case of the longer chain length of 9.79 Å for pentylamine, when bonded to opposing zirconium acid centers inside of the same lamella, an expansion could be expected, as observed for the subsequent *n*-alkylmonoamines.

Lazarin and Airoidi studied the intercalation of pyridine (py) and a-, b-, and c-picolines (a-, b-, and c-pic) into the crystalline structure of hydrated barium phenylphosphonate, $\text{Ba}[(\text{HO})\text{O}_2\text{PC}_6\text{H}_5]_2 \cdot 2\text{H}_2\text{O}$,²²⁶ which results in the formation of an intercalated material of the type:



The isotherms of intercalation present an increase in number of moles of amines intercalated with time or with the concentration of the supernatant. In all cases, intercalation causes a total saturation of the inorganic layered structure showing a decrease in the sequence $\text{py} > \text{c-pic} > \text{b-pic} > \text{a-pic}$.

Loss of the coordinated water in zinc phenylphosphonate monohydrate results in the dehydrated, also layered, zinc phenylphosphonate, $\text{Zn}(\text{O}_3\text{PC}_6\text{H}_5)$. When $\text{Zn}(\text{O}_3\text{PC}_6\text{H}_5) \cdot \text{H}_2\text{O}$ is in contact with liquid amine, the water molecule is replaced by amine producing the thermally stable $\text{Zn}(\text{O}_3\text{PC}_6\text{H}_5) \cdot (\text{RNH}_2)$ where the amine occupies the same coordination site as the water molecule in the monohydrate.²²⁹ The rate of intercalation of the amine into the dehydrated zinc phenylphosphonate depends on the size of the amine – the longer the alkyl chain, the slower the reaction. The interlayer spacing of zinc phenylphosphonate is 14.339(5) Å but layer expansion is observed for pentyl and longer chain amines and specifically an increase of about 4.2 Å occurred upon intercalation of heptylamine. Although the basic structures are similar, the interlayer distances do not uniformly increase as the size of the amine alkyl chain increases. This may be explained by the fact that the Zn coordination environment changes from six-coordinated to four-coordinated (tetrahedral), so “small” amines inserted do not protrude beyond the phenyl group within the interlayer space.

Dehydration of the copper phosphonates $\text{Cu}(\text{O}_3\text{PC}_6\text{H}_5) \cdot \text{H}_2\text{O}$ and $\text{Cu}(\text{O}_3\text{PCH}_3) \cdot \text{H}_2\text{O}$ leads to the formation of materials with evident amine adsorption where copper is in an unusual five-coordinate environment, occupying a water molecule bonded in the equatorial position of a distorted square pyramidal arrangement.¹⁷⁵ High dehydration temperatures are expected for these compounds, which are lower than the Co and Zn derivatives, a fact indicative of their relative instability. Anhydrous copper phosphonates are less crystalline than their monohydrates due to the increase in the interlayer spacing upon dehydration which may be caused by a reversible structural rearrangement due to the change in the coordination environment around Cu after dehydration. Like Co and Zn methylphosphonates, anhydrous copper methylphosphonate is quite reactive with primary amines forming amine intercalates through both solid–liquid and solid–gas reactions.²²⁸ Using solid–liquid method, the reaction begins instantaneously and reaches completion within a few hours followed by a phase change while drying in air. As the sample dries, the crystalline intercalated phase or phases converts to a final stable crystalline layered phase. The time required to complete the phase transformation during drying is proportional to the size of the primary amines.

Lima and Airoidi have studied the intercalation of crystalline calcium phenylphosphonate²³⁰ and calcium methylphosphonate²³¹ with *n*-alkylmonoamines. The chemical formula of the anhydrous calcium phosphonate²³² was previously proposed as $\text{Ca}(\text{O}_3\text{PC}_6\text{H}_5)_2$. Their investigations focused on the hydrated compound, $\text{Ca}(\text{HO}_3\text{PC}_6\text{H}_5)_2 \cdot 2\text{H}_2\text{O}$, in which two water molecules are coordinated to the inorganic backbone. When basic polar molecules are intercalated, these water molecules are gradually replaced.²³² During the intercalation process the guest molecules are oriented inside the free lamellar

cavity, causing an increase in the interlamellar distance to accommodate them inside the interlayer space.²³³ Thus, intercalation changes both guest and host properties. Calorimetric data, based on calorimetric titration²³⁴ and the breaking thin-glass ampoules,²³⁵ on intercalation between hydrated $\text{Ca}(\text{HO}_3\text{PC}_6\text{H}_5)_2 \cdot 2\text{H}_2\text{O}$ and anhydrous $\text{Ca}(\text{O}_3\text{PC}_6\text{H}_5)_2$ crystalline calcium phenylphosphonates and *n*-alkylmonoamines, $\text{CH}_3(\text{CH}_2)_n\text{NH}_2$ ($n=0-4, 7$), establish correlations between the physical properties of the host inorganic matrix and the guest molecules. The variation in enthalpy increases as the aliphatic amine chain length increases, as expressed by negative *G* values. For the guest molecule *n*-butylamine intercalated in the matrix in aqueous solution, the enthalpy values show an increase from the hydrated to anhydrous hosts, clearly a favorable condition of intercalation. This fact suggested that immersion of the anhydrous compound in water does not replace the solvent molecules in the lattice, as indicated by distinguishable enthalpy values. The enthalpy values obtained from calorimetric titration are linearly correlated with the number of carbon atoms on the aliphatic *n*-alkylmonoamines intercalated in water into $\text{Ca}(\text{HO}_3\text{PC}_6\text{H}_5)_2 \cdot 2\text{H}_2\text{O}$.

Inorganic titanium phenylphosphonate and titanium phenylarsonate, $\text{M}(\text{O}_3\text{XC}_6\text{H}_5)_2$, ($\text{M} = \text{Ti}$, $\text{X} = \text{P}$, As) matrices can also be used in the synthesis of such compounds. Intercalation of ethyl and propylamines, $\text{H}_3\text{C}(\text{CH}_2)_n\text{NH}_2$ ($n = 1, 2$) in ethanol or acetonitrile solvents causes a small change in lamellar space in both inorganic matrices.²³⁶ Thus, an evaluation of the capacity of intercalation of these two inorganic supports can be made. The most important effects (largest absolute magnitudes) are the type of inorganic material, the solvent, and the material mass.

Poojary and Clearfield have studied the intercalation of propyl-, butyl-, and pentylamine intercalates into both the hydrated and anhydrous zinc phenylphosphonates and were able to solve the intercalated structures from powder data.²³⁷ In all three intercalates the zinc atom exhibits a slightly distorted tetrahedral geometry. The coordination sites are occupied by three oxygen atoms from three different phosphonate groups and a nitrogen atom of the amine. Among the six bond angles around the metal atom, four have normal tetrahedral values while one is larger and the other is smaller possibly due to the spacial requirements for the positioning of the amine group. It may be noted that the distortion in the bond angles is less for the butylamine compound as compared to the other two intercalates. The phosphonate tetrahedron and the phenyl group show very regular bond parameters in all three compounds. The bond parameters involving the carbon atoms of the amine are also normal, although the values have larger errors which increase with the number of carbon atoms in the chain.

The structure of $\text{Cd}(\text{O}_3\text{PCH}_3) \cdot \text{H}_2\text{O}$ is composed by neutral slabs where Cd atoms are octahedrally coordinated by five oxygen atoms of phosphonate groups and a water molecule.²³⁸ This structure is similar to the one of $\text{Cd}(\text{O}_3\text{PC}_6\text{H}_5) \cdot \text{H}_2\text{O}$ as it concerns coordination environment around the Cd atoms and the plane arrangement of phosphonate groups and water molecule. A significant difference is that the CdO_6 octahedron in $\text{Cd}(\text{O}_3\text{PC}_6\text{H}_5) \cdot \text{H}_2\text{O}$

possesses a mirror symmetry whereas the CdO_6 octahedron in $\text{Cd}(\text{O}_3\text{PCH}_3) \cdot \text{H}_2\text{O}$ does not. Moreover, the stacking of the layers is different. Cadmium phenylphosphonate is isomorphous with manganese and zinc phenylphosphonates as they show the same unusual disorder of the phenyl rings whose positions are disordered among orientations. As a result, they reveal similarities in their dehydration and intercalation chemistry. It is interesting to note that $\text{Cd}(\text{O}_3\text{PCH}_3) \cdot \text{H}_2\text{O}$ crystallizes in the space group $\text{Pmn}2_1$ as divalent organophosphonates with the structural formula $\text{M}^{\text{II}}(\text{O}_3\text{PR}) \cdot \text{H}_2\text{O}$, while $\text{Cd}(\text{O}_3\text{PCH}_3) \cdot \text{H}_2\text{O}$ has no counterpart among the inorganic phosphates. Dehydration of the latter is likely to proceed topotactically and the compounds are formed with vapor and non-aqueous solution of amines including long-chain alkyl amines. Products can be formulated as $\text{Cd}(\text{O}_3\text{PCH}_3)(\text{RNH}_2)$ and their stability depends on the volatility of the amine involved. The intercalation compounds of lower molecular weight amines are not stable at room temperature while the compounds of higher amines are. Cadmium methylphosphonate intercalates amines with no branching at the α -carbon as the four methyl groups surrounding the site of the water molecule restrict the accessibility of the site sterically. Cadmium phenylphosphonate also reacts with amines due to structural changes associated with the reaction process which may proceed through a dissolution–recrystallization mechanism. Finally, it is interesting that weakly basic alkanethiols intercalate into the dehydrated cadmium phenylphosphonates with layer expansion.

Besides amines, other molecules can also be intercalated into the metal phosphonate structure. For example, Mao *et al.* have reported the intercalation of 1,3,5-benzenetricarboxylate (H_3BTC) into the structure of lead bisphosphonate, where the phosphonate is $\text{C}_6\text{H}_5\text{CH}_2\text{N}(\text{CH}_2\text{PO}_3\text{H}_2)_2$ (H_4L).²³⁹ Hydrothermal reaction of H_4L with lead(II) carbonate in the presence of butanedicarboxylic acid results in the materials $\text{Pb}_3\text{L}(\text{H}_2\text{L}) \cdot 1.5\text{H}_2\text{O}$ with different layered structures. When H_3BTC is used instead of butanedicarboxylic acid, a novel lead(II) biphosphonate, with the molecular formula $\text{Pb}_3(\text{HL})_2 \cdot 2(\text{H}_3\text{BTC}) \cdot 2\text{H}_2\text{O}$, is isolated with a porous 3D network.

Seven new ethylenediphosphonates with the formula $[\text{A}\{\text{HO}_3\text{P}(\text{CH}_2)_2\text{PO}_3\text{H}_2\}]$ ($\text{A} = \text{Li}, \text{Na}, \text{K}, \text{Rb}, \text{Cs}, \text{Tl}, \text{and } \text{NH}_4$) have been synthesized and characterized by single-crystal X-ray diffraction, infrared spectroscopy, and thermal studies.²⁴⁰ They have four types of 3D structures, with variations in the coordination of the A^+ ions. All of them are solid Brønsted acids that undergo room temperature, acid–base intercalation reactions with ammonia.

The 2D layered material $\text{Ca}(\text{HDTMP}) \cdot 2\text{H}_2\text{O}$ exhibits interesting NH_3 absorption properties.²⁴¹ The basic building block for this phosphonate consists of an eight-membered ring formed by Ca^{2+} chelation by two phosphonate oxygens (from two different phosphonate groups) and the organic ligand. The latter is located *within* the layers, which are held together by H-bonding. Thermal treatment and subsequent exposure to NH_3 and/or H_2O vapors led to four new compounds showing high storage capacity of guest species between the layers, up to 10 $\text{H}_2\text{O}/\text{NH}_3$ molecules, and a maximum unit cell volume increase of 55% (Figure 14.35).

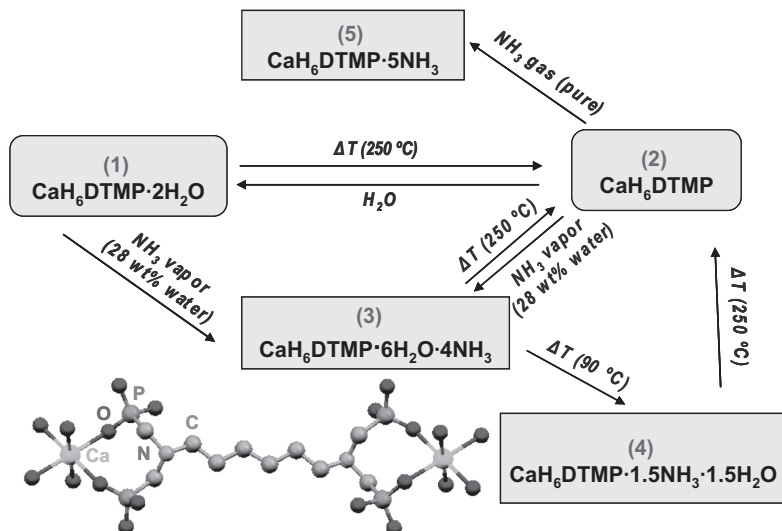


Figure 14.35 Interconversions between the reported calcium tetraphosphonate hybrids due to incorporation/removal of host molecules. The basic structural unit for this family is also shown. (Reproduced with permission from ref. 240.)

The structural analysis revealed that uptake/removal of guest species (H_2O and NH_3) induces significant changes in the framework, not only by changing the interlayer distances, but also through important conformational changes of the organic ligand (Figure 14.36). Anisotropic breathing motion could be quantified by the changes of unit cell dimensions and ligand arrangements in four crystalline derivatives. Complete characterization revealed the existence of interconversion reactions between the different phases upon gas uptake and release.

Due to the intense interest lately in ammonia storage, we will add a word on its storage in covalent organic frameworks (COFs). These are porous crystalline materials composed of light elements linked by strong covalent bonds. A number of these materials contain a high density of Lewis acid boron sites that can strongly interact with Lewis basic guests, which makes them ideal for the storage of corrosive chemicals such as ammonia. We found that a member of the covalent organic framework family, COF-10, shows the highest uptake capacity (15 mol kg^{-1} , 298 K, 1 bar) of any porous material, including microporous 13X zeolite (9 mol kg^{-1}), Amberlyst 15 (11 mol kg^{-1}) and mesoporous silica, MCM-41 (7.9 mol kg^{-1}).²⁴² Notably, ammonia can be removed from the pores of COF-10 by heating samples at $200\text{ }^\circ\text{C}$ under vacuum. In addition, repeated adsorption of ammonia into COF-10 causes a shift in the interlayer packing, which reduces its apparent surface area to nitrogen. However, owing to the strong Lewis acid–base interactions, the total uptake capacity of ammonia and the structural integrity of the COF are maintained after several cycles of adsorption/desorption.

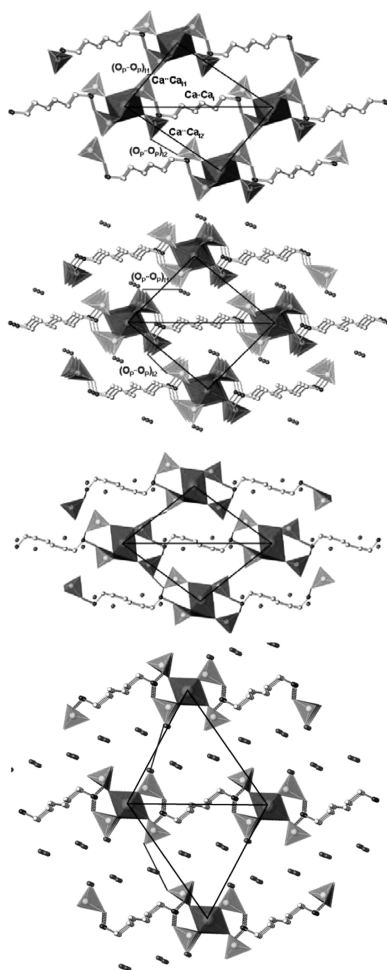


Figure 14.36 Structures of the hybrids showing the breathing with the guest species uptake. From top to bottom: (2), (1), (4), and (3). For the numbering scheme, see Figure 14.35. (Reproduced with permission from ref. 240.)

References

1. A. Clearfield, *Chem. Mater.*, 1998, **10**, 2801.
2. K. Maeda, *Microporous Mesoporous Mater.*, 2004, **73**, 47.
3. K. D. Demadis, in *Solid State Chemistry Research Trends*, ed. R. W. Buckley, Nova Science Publishers, New York, 2007, p. 109.
4. C. V. K. Sharma and A. Clearfield, *J. Am. Chem. Soc.*, 2000, **122**, 4394.
5. A. Clearfield, *Prog. Inorg. Chem.*, 1998, **47**, 371.
6. A. Vioux, L. Le Bideau, P. Hubert Mutin and D. Leclercq, *Top. Curr. Chem.*, 2004, **232**, 145.
7. A. H. Mahmoudkhani and V. Langer, *Phosphorus Sulfur Silicon*, 2002, **177**, 2941.

8. A. H. Mahmoudkhani and V. Langer, *J. Mol. Struct.*, 2002, **609**, 97.
9. A. N. Lazar, A. Navaza and A. W. Coleman, *Chem. Commun.*, 2004, 1052.
10. A. H. Mahmoudkhani and V. Langer, *Cryst. Growth Des.*, 2002, **2**, 21.
11. Z.-Y. Du, A. V. Prosvirin and J.-G. Mao, *Inorg. Chem.*, 2007, **46**, 9884.
12. Z.-Y. Du, H.-B. Xu and J.-G. Mao, *Inorg. Chem.*, 2006, **45**, 6424.
13. B.-P. Yang and J.-G. Mao, *Inorg. Chem.*, 2005, **44**, 566.
14. C. Lei, J.-G. Mao, Y.-Q. Sun, H.-Y. Zeng and A. Clearfield, *Inorg. Chem.*, 2003, **42**, 6157.
15. A. K. Cheetham, G. Ferey and T. Loiseau, *Angew. Chem. Int. Ed. Engl.*, 1999, **38**, 3268.
16. P. M. Forster and A. K. Cheetham, *Top. Catal.*, 2003, **24**, 79.
17. C. A. Merrill and A. K. Cheetham, *Inorg. Chem.*, 2007, **46**, 278.
18. S. H. Jhung, J. W. Yoon, J.-S. Hwang, A. K. Cheetham and J.-S. Chang, *Chem. Mater.*, 2005, **17**, 4455.
19. C. A. Merrill and A. K. Cheetham, *Inorg. Chem.*, 2005, **44**, 5273.
20. M. M. Gomez-Alcantara, A. Cabeza, M. Martinez-Lara, M. A. G. Aranda, R. Suau, N. Bhuvanesh and A. Clearfield, *Inorg. Chem.*, 2004, **43**, 5283.
21. A. Cabeza, O. Y. Xiang, C. V. K. Sharma, M. A. G. Aranda, S. Bruque and A. Clearfield, *Inorg. Chem.*, 2002, **41**, 2325.
22. A. Cabeza, M. A. G. Aranda and S. Bruque, *J. Mater. Chem.*, 1999, **9**, 571.
23. A. Turner, P.-A. Jaffres, E. J. MacLean, D. Villemin, V. McKee and G. B. Hix, *J. Chem. Soc. Dalton Trans.*, 2003, 1314.
24. G. B. Hix, D. S. Wragg, P. A. Wright and R. E. Morris, *J. Chem. Soc. Dalton Trans.*, 1998, 3359.
25. A. Turner, B. M. Kariuki, M. Tremayne and E. J. MacLean, *J. Mater. Chem.*, 2002, **12**, 3220.
26. N. Zakowsky, G. B. Hix and R. E. Morris, *J. Mater. Chem.*, 2000, **10**, 2375.
27. N. Stock and T. Bein, *Angew. Chem. Int. Ed. Engl.*, 2004, **43**, 749.
28. S. Bauer and N. Stock, *Angew. Chem. Int. Ed. Engl.*, 2007, **46**, 6857.
29. P. M. Forster, N. Stock and A. K. Cheetham, *Angew. Chem. Int. Ed. Engl.*, 2005, **44**, 7608.
30. S. Bauer, T. Bein and N. Stock, *J. Solid State Chem.*, 2006, **179**, 145.
31. B. A. Breeze, M. Shanmugam, F. Tuna and R. E. P. Winpenny, *Chem. Commun.*, 2007, 5185.
32. S. Langley, M. Helliwell, J. Raftery, E. I. Tolis and R. E. P. Winpenny, *Chem. Commun.*, 2004, 142.
33. V. Baskar, M. Shanmugam, E. C. Sañudo, M. Shanmugam, D. Collison, E. J. L. McInnes, Q. Wei and R. E. P. Winpenny, *Chem. Commun.* 2007, 37.
34. A. Harrison, D. K. Henderson, P. A. Lovatt, A. Parkin, P. A. Tasker and R. E. P. Winpenny, *Dalton Trans.* 2003, 4271.
35. C. Serre, J. A. Groves, P. Lightfoot, A. M. Z. Slawin, P. A. Wright, N. Stock, T. Bein, M. Haouas, F. Taulelle and G. Ferey, *Chem. Mater.*, 2006, **18**, 1451.

36. G. Ferey, C. Mellot-Draznieks, C. Serre and F. Millange, *Acc. Chem. Res.*, 2005, **38**, 217.
37. C. Serre, C. Lorentz, F. Taulelle and G. Ferey, *Chem. Mater.*, 2003, **15**, 2328.
38. K. Barthelet, M. Nogues, D. Riou and G. Ferey, *Chem. Mater.*, 2002, **14**, 4910.
39. G. Alberti, M. Casciola, U. Costantino and R. Vivani, *Adv. Mater.*, 1996, **8**, 291.
40. R. Vivani, G. Alberti, F. Costantino and M. Nocchetti, *Microporous Mesoporous Mater.*, 2008, **107**, 58.
41. R. Vivani, F. Costantino, U. Costantino and M. Nocchetti, *Inorg. Chem.*, 2006, **45**, 2388.
42. U. Costantino, M. Nocchetti and R. Vivani, *J. Am. Chem. Soc.*, 2002, **124**, 8428.
43. K. D. Demadis and S. D. Katarachia, *Phosphorus Sulfur Silicon*, 2004, **179**, 627.
44. K. D. Demadis and P. Lykoudis, *Bioinorg. Chem. Appl.*, 2005, **3**, 135.
45. K. D. Demadis, *Phosphorus Sulfur Silicon*, 2006, **181**, 167.
46. K. D. Demadis and E. Mavredaki, *Env. Chem. Lett.*, 2005, **3**, 127.
47. S. J. Dyer, C. E. Anderson and G. M. Graham, *J. Pet. Sci. Eng.*, 2004, **43**, 259.
48. J. E. Oddo and M. B. Tomson, *Appl. Geochem.*, 1990, **5**, 527.
49. J. J. Xiao, A. T. Kan and M. B. Tomson, *Langmuir*, 2001, **17**, 4668.
50. S. J. Friedfeld, S. He and M. B. Tomson, *Langmuir*, 1998, **14**, 3698.
51. V. Tantayakom, H. S. Fogler, P. Charoensirithavorn and S. Chavadej, *Cryst. Growth Des.*, 2005, **5**, 329.
52. F. H. Browning and H. S. Fogler, *AIChE J.*, 1996, **42**, 2883.
53. R. Pairat, C. Sumeath, F. H. Browning and H. S. Fogler, *Langmuir*, 1997, **13**, 1791.
54. V. Tantayakom, H. S. Fogler, F. F. de Moraes, M. Bualuang, S. Chavadej and P. Malakul, *Langmuir*, 2004, **20**, 2220.
55. A.-L. Penard, F. Rossignol, H. S. Nagaraja, C. Pagnoux and T. Chartier, *Eur. J. Ceram. Soc.*, 2005, **25**, 1109.
56. M. J. Pearse, *Min. Eng.*, 2005, **18**, 139.
57. I. Sekine, T. Shimode and M. Yuasa, *Ind. Eng. Chem. Res.*, 1992, **31**, 434.
58. B. Mosayebi, M. Kazemeini and A. Badakhshan, *Br. Corr. J.*, 2002, **37**, 217.
59. Yu I. Kouznetsov, *Prot. Met.*, 2001, **37**, 434.
60. Yu V. Balaban-Irmenin, A. M. Rubashov and N. G. Fokina, *Prot. Met.*, 2006, **42**, 133.
61. J. L. Fang, Y. Li, X. R. Ye, Z. W. Wang and Q. Liu, *Corrosion*, 1993, **49**, 266.
62. A. Paszternák, S. Stichleitner, I. Felhősi, Z. Keresztes, F. Nagy, E. Kuzmann, A. Vértés, Z. Homonnay, G. Pető and E. Kálmán, *Electrochim. Acta*, 2007, **53**, 337.
63. *Biogeochemistry of Chelating Agents*, ed. B. Nowack, J. M. Van Briessen, J. M. ACS Symposium Series, ACS, Washington DC, 2003, Vol. 910.

64. T. P. Knepper, *Trends Anal. Chem.*, 2003, **22**, 708.
65. K. Miyazaki, T. Horibe, J. M. Antonucci, S. Takagi and L. C. Chow, *Dent. Mater.*, 1993, **9**, 46.
66. M. Atai, M. Nekoomanesh, S. A. Hashemi and S. Amani, *Dent. Mater.*, 2004, **20**, 663.
67. J. W. Nicholson and G. Singh, *Biomaterials*, 1996, **17**, 2023.
68. H. Tschernitschek, L. Borchers and W. Geurtsen, *J. Prosth. Dent.*, 2006, **96**, 12.
69. F. Cheng and E. Oldfield, *J. Med. Chem.*, 2004, **47**, 5149.
70. C. Temperini, A. Innocenti, A. Guerri, A. Scozzafava, S. Rusconi and C. T. Supuran, *Bioorg. Med. Chem. Lett.*, 2007, **17**, 2210.
71. E. Davini, C. Di Leo, F. Norelli and P. Zappelli, *J. Biotechnol.*, 1993, **28**, 321.
72. M. Bottrill, L. Kwok and N. J. Long, *Chem. Soc. Rev.*, 2006, **35**, 557.
73. I. G. Finlay, M. D. Mason and M. Shelley, *Lancet Oncol.*, 2005, **6**, 392.
74. V. Kubicek, J. Rudovsky, J. Kotek, P. Hermann, L. Vander Elst, R. N. Muller, Z. I. Kolar, H. T. Wolterbeek, J. A. Peters and I. Lukeš, *J. Am. Chem. Soc.*, 2005, **127**, 16477.
75. H. Kung, R. Ackerhalt and M. Blau, *J. Nucl. Med.*, 1978, **19**, 1027.
76. S. S. Padalecki and T. A. Guise, *Breast Cancer Res.*, 2001, **4**, 35.
77. V. Stresing, F. Daubiné, I. Benzaid, H. Mönkkönen and P. Clézardin, *Cancer Lett.*, 2007, **257**, 16.
78. R. Layman, K. Olson and C. Van Poznak, *Hematol. Oncol. Clinics North Am.*, 2007, **21**, 341.
79. A. Clearfield, *Curr. Opin. Solid State Mater. Sci.*, 2002, **6**, 495.
80. A. Clearfield, *Curr. Opin. Solid State Mater. Sci.*, 1996, **1**, 268.
81. E. Barouda, K. D. Demadis, S. Freeman, F. Jones and M. I. Ogden, *Cryst. Growth Des.*, 2007, **7**, 321.
82. K. Popov, H. Rönkkömäki and L. H. J. Lajunen, *Pure Appl. Chem.*, 2001, **73**, 1641.
83. M. Dyba, M. Jezowska-Bojczuk, E. Kiss, T. Kiss, H. Kozłowski, Y. Leroux and D. El Manouni, *J. Chem. Soc. Dalton Trans.*, 1996, 1119.
84. E. Gumienna-Kontecka, J. Jezierska, M. Lecouvey, Y. Leroux and H. Kozłowski, *J. Inorg. Biochem.*, 2002, **89**, 13.
85. E. Gumienna-Kontecka, R. Silvagni, R. Lipinski, M. Lecouvey, F. C. Marincola, G. Crisponi, V. M. Nurchi, Y. Leroux and H. Kozłowski, *Inorg. Chim. Acta*, 2002, **339**, 111.
86. E. Matczak-Jon, B. Kurzak, A. Kamecka and P. Kafarski, *Polyhedron*, 2002, **21**, 321.
87. B. Boduszek, M. Dyba, M. Jezowska-Bojczuk, T. Kiss and H. Kozłowski, *J. Chem. Soc. Dalton Trans.*, 1997, 973.
88. B. Kurzak, A. Kamecka, K. Kurzak, J. Jezierska and P. Kafarski, *Polyhedron*, 1998, **17**, 4403.
89. E. Matczak-Jon, B. Kurzak, A. Kamecka, W. Sawka-Dobrowolska and P. Kafarski, *J. Chem. Soc. Dalton Trans.*, 1999, 3627.

90. G. V. Polyanchuk, L. M. Shkol'nikova, M. V. Rudomino, N. M. Dyatlova and S. S. Makarevich, *J. Struct. Chem.*, 1985, **26**, 586.
91. G. B. Hix, V. Caignaert, J.-M. Rueff, L. Le Pluart, J. E. Warren and P.-A. Jaffrès, *Cryst. Growth Des.*, 2007, **7**, 208.
92. K. M. E. Jones, A. H. Mahmoudkhani, B. D. Chandler and G. K. H. Shimizu, *CrystEngComm*, 2006, **8**, 303.
93. K. D. Demadis, R. G. Raptis and P. Baran, *Bioinorg. Chem. Appl.*, 2005, **3**, 119.
94. K. D. Demadis, E. Barouda, H. Zhao and R. G. Raptis, *Polyhedron*, 2009, **28**, 3361.
95. S. Lodhia, A. Turner, M. Papadaki, K. D. Demadis and G. B. Hix, *Cryst. Growth Des.*, 2009, **9**, 1811.
96. K. D. Demadis, S. D. Katarachia, H. Zhao, R. G. Raptis and P. Baran, *Cryst. Growth Des.*, 2006, **6**, 836.
97. K. D. Demadis, A. Panera, unpublished results.
98. K. D. Demadis, M. Papadaki, R. G. Raptis and H. Zhao, *J. Solid State Chem.*, 2008, **181**, 679.
99. K. D. Demadis, M. Papadaki, R. G. Raptis and H. Zhao, *Chem. Mater.*, 2008, **20**, 4835.
100. J. Yang, J.-F. Ma, G.-L. Zheng, L. Li, F.-F. Li, Y.-M. Zhang and J.-F. Liu, *J. Solid State Chem.*, 2003, **174**, 116.
101. R. Murugavel, S. Kuppaswamy and S. Randoll, *Inorg. Chem.*, 2008, **47**, 6028.
102. M. Tuikka, M. Haukka and M. Ahlgren, *Solid State Sci.*, 2007, **9**, 535.
103. S. Bauer, H. Muller, T. Bein and N. Stock, *Inorg. Chem.*, 2005, **44**, 9464.
104. D. S. Sagatys, C. Dahlgren, G. Smith, R. C. Bott and J. M. White, *J. Chem. Soc. Dalton Trans.*, 2000, 3404.
105. H. S. Martínez-Tapia, A. Cabeza, S. Bruque, P. Pertierra, S. García-Granda and M. A. G. Aranda, *J. Solid State Chem.*, 2000, **151**, 122.
106. C.-Y. Cheng and K.-J. Lin, *Acta Crystallogr.*, 2006, **C62**, m363.
107. R. Fu, S. Xia, S. Xiang, S. Hu and X. Wu, *J. Solid State Chem.*, 2004, **177**, 4626.
108. K. D. Demadis, M. Papadaki, M. A. G. Aranda, A. Cabeza, P. Olivera-Pastor and Y. Sanakis, *Cryst. Growth Des.*, 2010, **10**, 357.
109. R. M. P. Colodrero, P. Olivera-Pastor, A. Cabeza, M. Papadaki, K. D. Demadis and M. A. G. Aranda, *Inorg. Chem.*, 2010, **49**, 761.
110. G.-L. Zheng, J.-F. Ma and J. Yang, *J. Chem. Res.* 2004, 387.
111. S.-J. Fu, C.-Y. Cheng and K.-J. Lin, *Acta Crystallogr.*, 2007, **C63**, m368.
112. W. R. Gemmill, M. D. Smith and B. A. Reisner, *J. Solid State Chem.*, 2005, **178**, 2658.
113. O. H. S. Gustschke, D. J. Price, A. K. Powell and P. T. Wood, *Angew. Chem. Int. Ed. Engl.*, 1999, **38**, 1088.
114. A. Distler, D. L. Lohse and S. C. Sevov, *J. Chem. Soc. Dalton Trans.*, 1999, 1805.
115. R. LaDuca, D. Rose, J. R. D. DeBord, R. C. Haushalter, C. J. O'Connor and J. Zubieta, *J. Solid State Chem.*, 1996, **123**, 408.

116. P. Rabu, P. Janvier and B. Bujoli, *J. Mater. Chem.*, 1999, **9**, 1323.
117. D. L. Lohse and S. C. Sevov, *Angew. Chem. Int. Ed. Engl.*, 1997, **36**, 1619.
118. F.-N. Shi, F. A. Almeida Paz, P. Girginova, J. Rocha, V. S. Amaral, J. Klinowski and T. Trindade, *J. Mol. Struct.*, 2006, **789**, 200.
119. P. Yin, S. Gao, Z.-M. Wang, C.-H. Yan, L.-M. Zheng and X.-Q. Xin, *Inorg. Chem.*, 2005, **44**, 2761.
120. N. Stock, M. Rauscher and T. Bein, *J. Solid State Chem.*, 2004, **177**, 642.
121. K. D. Demadis, S. D. Katarachia and M. Koutmos, *Inorg. Chem. Commun.*, 2005, **8**, 254.
122. J.-G. Mao, Z. Wang and A. Clearfield, *New J. Chem.*, 2002, **26**, 1010.
123. K. D. Demadis, C. Mantzaridis, R. G. Raptis and G. Mezei, *Inorg. Chem.*, 2005, **44**, 4469.
124. J. Li, D.-P. Dong, C.-Y. Huang, Z.-G. Sun and Y.-Y. Zhu, *Acta Crystallogr.*, 2007, **E63**, m2348.
125. E. M. Bauer, C. Bellitto, P. Imperatori, G. Righini, M. Colapietro, G. Portalone and C. J. Gomez-Garcia, *Inorg. Chem.*, 2010, **49**, 7472.
126. L. R. Olano, H. T. Tran, J. T. Mague and D. A. Knight, *J. Chem. Crystallogr.*, 2003, **33**, 497.
127. A. Cabeza, S. Bruque, A. Guagliardi and M. A. G. Aranda, *J. Solid State Chem.*, 2001, **160**, 278.
128. K. Maeda, Y. Hashiguchi, Y. Kiyozumi and F. Mizukami, *Bull. Chem. Soc. Jpn.*, 1997, **70**, 345.
129. H. G. Harvey, M. P. Attfield, *Solid State Sci.*, 2006, **8**, 404.
130. R. Murugavel, N. Gogoi and R. Clerac, *Inorg. Chem.*, 2009, **48**, 646.
131. B. Adair, S. Natarajan and A. K. Cheetham, *J. Mater. Chem.*, 1998, **8**, 1477.
132. A. Subbiah, N. Bhuvanesh and A. Clearfield, *J. Solid State Chem.*, 2005, **178**, 1321.
133. D. E. Lansky, P. Y. Zavalij and S. R. J. Oliver, *Acta Crystallogr.*, 2001, **C57**, 1051.
134. N. Stock, N. Guillou, T. Bein and G. Férey, *Solid State Sci.*, 2003, **5**, 629.
135. B. Zhang, D. M. Poojary and A. Clearfield, *Inorg. Chem.*, 1998, **37**, 249.
136. D. M. Poojary and A. Clearfield, *J. Organomet. Chem.*, 1996, **512**, 237.
137. D. M. Poojary, L. A. Vermeulen, E. Vicenzi, A. Clearfield and M. E. Thompson, *Chem. Mater.*, 1994, **6**, 1845.
138. R. Vivani, U. Costantino and M. Nocchetti, *J. Mater. Chem.*, 2002, **12**, 3254.
139. R. Vivani, F. Costantino, M. Nocchetti and G. D. Gatta, *J. Solid State Chem.*, 2004, **177**, 4013.
140. D. M. Poojary, C. Bhardwaj and A. Clearfield, *J. Mater. Chem.*, 1995, **5**, 171.
141. P. P. Charpin, M. Lance, M. Nierlich, D. Vigner, M.-R. Lee, J.-P. Silvestre and N. Q. Dao, *Acta Crystallogr.*, 1988, **C44**, 990.
142. A. M. Beaty, B. A. Helfrich, G. A. Hogan and B. A. Reed, *Cryst. Growth Des.*, 2006, **6**, 122.

143. K. D. Demadis, Z. Anagnostou and H. Zhao, *ACS-Appl. Mater. Interf.*, 2009, **1**, 35.
144. S. M. Hawxwell, H. Adams and L. Brammer, *Acta Crystallogr.*, 2006, **B62**, 808.
145. K. M. Fromm, *Coord. Chem. Rev.*, 2008, **252**, 856.
146. R. Robson, *Dalton Trans.*, 2008, 5113.
147. A. U. Czaja, N. Trukhan and U. Muller, *Chem. Soc. Rev.*, 2009, **38**, 1284.
148. M. Kurmoo, *Chem. Soc. Rev.*, 2009, **38**, 1353.
149. G. Ferey, *Dalton Trans.*, 2009, 4400.
150. N. L. Rosi, M. Eddaoudi, J. Kim, M. O'Keeffe and O. M. Yaghi, *Cryst-EngComm*, 2002, **4**, 401.
151. K. D. Demadis, J. D. Sallis, R. G. Raptis and P. Baran, *J. Am. Chem. Soc.*, 2001, **123**, 10129.
152. J. Jokiniemi, S. Peräniemi, J. J. Vepsäläinen and M. Ahlgrein, *Cryst-EngComm*, 2008, **10**, 1011.
153. P. A. Turhanen, K. D. Demadis, S. Peräniemi and J. J. Vepsäläinen, *J. Org. Chem.*, 2007, **72**, 1468.
154. (a) H. Kumpulainen, R. Saari, M. Lehtonen, J. Rautio, T. Järvinen and J. Vepsäläinen, *Tetrahedron Lett.*, 2006, **47**, 2003; (b) R. Murugavel, A. Choudhury, M. G. Walawalkar, R. Pothiraja and C. N. R. Rao, *Chem. Rev.*, 2008, **108**, 3549.
155. S. Natarajan and P. Mahata, *Curr. Opin. Solid State Mater. Sci.*, 2009, **13**, 46.
156. L.-S. Long, *CrystEngComm*, 2010, **12**, 1354.
157. R. G. Lin, L. S. Long, R. B. Huang and L. S. Zheng, *Inorg. Chem. Commun.*, 2007, **10**, 1257.
158. S. J. Dalgarno, J. L. Atwood and C. L. Raston, *Cryst. Growth Des.*, 2006, **6**, 174.
159. C. Liu, F. Luo, W. P. Liao, D. Q. Li, X. F. Wang and R. Dronskowski, *Cryst. Growth Des.*, 2007, **7**, 2282.
160. S. J. Dalgarno, M. J. Hardie and C. L. Raston, *Cryst. Growth Des.*, 2004, **4**, 227.
161. A. Cabeza, M. A. G. Aranda, S. Bruque, D. M. Poojary, A. Clearfield and J. Sanz, *Inorg. Chem.*, 1998, **37**, 4168.
162. J. Le Bideau, C. Payen, P. Palvadeau and B. Bujoli, *Inorg. Chem.*, 1994, **33**, 4885.
163. R. Fu, H. Zhang, L. Wang, S. Hu, Y. Li, X. Huang and X. Wu, *Eur. J. Inorg. Chem.* 2005, 3211.
164. Q.-H. Zhao, L. Dua and R.-B. Fang, *Acta Crystallogr.*, 2006, **E62**, m219.
165. R. Fu, S. Hu and X. Wu, *Dalton Trans.*, 2009, 9843.
166. Z.-G. Sun, D.-P. Dong, J. Li, L.-Y. Cui, Y.-Y. Zhu, J. Zhang, Y. Zhao, W.-S. You and Z.-M. Zhu, *J. Coord. Chem.*, 2007, **60**, 2541.
167. Y.-Y. Zhang, M.-H. Zeng, Y. Qi, S.-Y. Sang and Z.-M. Liu, *Inorg. Chem. Commun.*, 2007, **10**, 33.
168. J. Li, L. Meng, Z.-G. Sun, L.-Y. Cui, J. Zhang, Y.-Y. Zhu, D.-P. Dong, H. Chen, W.-S. You and Z.-M. Zhu, *Inorg. Chem. Commun.*, 2007, **10**, 535.

169. Z.-Y. Du, J.-J. Huang, Y.-R. Xie and H.-R. Wen, *J. Mol. Struct.*, 2009, **919**, 112.
170. V. Chandrasekhar, T. Senapati and R. Clérac, *Eur. J. Inorg. Chem.* 2009, 1640.
171. V. Chandrasekhar, R. Azhakar, T. Senapati, P. Thilagar, S. Ghosh, S. Verma, R. Boomishankar, A. Steiner and P. Kogerler, *Dalton Trans.*, 2008, 1150.
172. K. D. Demadis and D. Varouchas, *unpublished results*.
173. G. Alberti, U. Constantino, S. Allulli and N. Tomassini, *J. Inorg. Nucl. Chem.*, 1978, **40**, 1113.
174. G. Cao, H.-G. Hong and T. E. Mallouk, *Acc. Chem. Res.*, 1992, **25**, 422.
175. Y. P. Zhang and A. Clearfield, *Inorg. Chem.*, 1992, **31**, 2821.
176. M. E. Thompson, *Chem. Mater.*, 1994, **6**, 1168.
177. K. Maeda and F. Mizukami, *Catal. Surv. Jpn.*, 1999, **3**, 119.
178. K. Yamamoto, Y. Sakata, Y. Nohara, Y. Takahashi and T. Tatsumi, *Science*, 2003, **300**, 470.
179. G. Gunasekaran, R. Natarajan, V. S. Muralidharan, N. Palaniswamy and B. V. Appa Rao, *Anti-Corr. Meth. Mater.*, 1997, **44**(4), 248.
180. S. M. Cohen, *Corrosion*, 1995, **51**, 71.
181. S. Rajendran, B. V. Appa Rao and N. Palaniswamy, *Anti-Corr. Meth. Mater.*, 1999, **46**(1), 23.
182. E. Kalman, I. Lukovits and G. Palinkas, *ACH-Models in Chemistry*, 1995, **132**, 527.
183. M. Papadaki and K. D. Demadis, *Commun. Inorg. Chem.*, 2009, **30**, 89.
184. B. P. Boffardi, in *Reviews on Corrosion Inhibitor Science and Technology*, ed. A. Raman, P. Labine, NACE International, Houston, TX, 1993, p. 6.
185. K. D. Demadis, M. Papadaki and I. Cisarova, *ACS-Appl. Mater. Interf.*, 2010, **2**, 1814.
186. K. D. Demadis, P. Lykoudis, R. G. Raptis and G. Mezei, *Cryst. Growth Des.*, 2006, **6**, 1064.
187. M. Benabdellah, A. Dafali, B. Hammouti, A. Aouniti, M. Rhomari, A. Raada, O. Sehaji and J. J. Robin, *Chem. Eng. Commun.*, 2007, **194**, 1328.
188. K. D. Demadis, E. Barouda, N. Stavgianoudaki and H. Zhao, *Cryst. Growth Des.*, 2009, **9**, 1250.
189. K. D. Demadis, E. Barouda, R. G. Raptis and H. Zhao, *Inorg. Chem.*, 2009, **48**, 819.
190. J. Menke, *NACE Conference 1999*, Corrosion/99, Paper number 503.
191. Editorial, *Chem. Process.* 2002, December, 11.
192. K. D. Demadis, B. Yang, P. R. Young, D. L. Kouznetsov, D. G. Kelley, in *Advances in Crystal Growth Inhibition Technologies*, ed. Z. Amjad, Plenum Publishing Corporation, New York, 2000, Chapter 16, p. 215.
193. K. D. Demadis, in *Compact Heat Exchangers and Enhancement Technology for the Process Industries*, ed. R. K. Shah, Begell House Inc. New York, 2003, p. 483.
194. H. Li, M. Eddaoudi, M. O'Keeffe and O. M. Yaghi, *Nature*, 1999, **402**, 276.

195. G. Ferey, C. Mellot-Draznieks, C. Serre and F. Millange, *Acc. Chem. Res.*, 2005, **38**, 217.
196. S. S. Y. Chui, J. P. H. Charmant, A. G. Orpen and I. D. Williams, *Science*, 1999, **283**, 1148.
197. K. S. Park, Z. Ni, A. P. Côté, J. Y. Choi, R. D. Huang, F. J. Uribe-Romo, H. K. Chae, M. O’Keeffe and O. M. Yaghi, *Proc. Natl. Acad. Sci. USA*, 2006, **103**, 10186.
198. R. Matsuda, R. Kituara, S. Kitagawa, Y. Kubota, R. V. Belosludov, T. C. Kobayashi, H. Sakamoto, T. Chiba, M. Takata, Y. Kawazoe and Y. Mita, *Nature*, 2005, **436**, 238.
199. (a) R. Vaidhyathan, D. Bradshaw, J. N. Rebilly, J. P. Barrio, J. A. Gould, N. G. Berry and M. J. Rosseinsky, *Angew. Chem. Int. Ed. Engl.*, 2006, **45**, 6495; (b) I. Imaz, M. Rubio-Martinez, J. An, I. Sole-Font, N. L. Rosi and D. Maspoch, *Chem. Commun.*, 2011, **47**, 7287.
200. J. A. Groves, S. R. Miller, S. J. Warrender, C. Mellot-Draznieks, P. Lightfoot and P. A. Wright, *Chem. Commun.*, 2006, 3305.
201. S. R. Miller, G. M. Pearce, P. A. Wright, F. Bonino, S. Chavan, S. Bordiga, I. Margiolaki, N. Guillou, G. Ferey, S. Bourrelly and P. L. Liewellyn, *J. Am. Chem. Soc.*, 2008, **130**, 15967.
202. J. M. Tylor, A. H. Mahmoudkhani and G. K. H. Shimizu, *Angew. Chem. Int. Ed. Engl.*, 2007, **46**, 795.
203. E. Brunet, H. M. H. Alhendawi, C. Cerro, M. J. de la Mata, O. Juans and J. C. Rodriguez-Ubis, *Angew. Chem. Int. Ed. Engl.*, 2006, **45**, 6918.
204. G. Alberti, R. Vivani, F. Marmottini and P. Zappelli, *J. Porous Mater.*, 1998, **5**, 205.
205. A. Clearfield and Z. K. Wang, *J. Chem. Soc. Dalton Trans.*, 2002, 2937.
206. E. Brunet, C. Cerro, O. Juanes, J. C. Rodriguez-Ubis and A. Clearfield, *J. Mater. Sci.*, 2008, **43**, 1155.
207. M. Plabst, L. B. McCusker and T. Bein, *J. Am. Chem. Soc.*, 2009, **131**, 18112.
208. J. Wu, H. Hou, H. Han and Y. Fan, *Inorg. Chem.*, 2007, **46**, 7960.
209. S. A. Dalrymple and G. K. H. Shimizu, *Chem. Eur. J.*, 2002, **8**, 3010.
210. A. I. Bortun, L. N. Bortun, A. Clearfield, S. A. Khainakov and J. R. García, *Solv. Extr. Ion Exch.*, 1998, **16**, 651.
211. A. Jayswal and U. Chudasama, *Turk. J. Chem.*, 2008, **32**, 63.
212. T.-Y. Ma, X.-J. Zhang and Z.-Y. Yuan, *J. Mater. Sci.*, 2009, **44**, 6775.
213. X.-J. Zhang, T.-Y. Ma and Z.-Y. Yuan, *J. Mater. Chem.*, 2008, **18**, 2003.
214. T.-Y. Ma, X.-J. Zhang, G.-S. Shao, J.-L. Cao and Z.-Y. Yuan, *J. Phys. Chem. C*, 2008, **112**, 3090.
215. A. Popa, C.-M. Davidescu, N. Petru, I. Gheorghe, A. Katsaros and K. D. Demadis, *Ind. Eng. Chem. Res.*, 2008, **47**, 2010.
216. M. Smolik, A. Jakóbič-Kolon and M. Porański, *Hydrometallurgy*, 2009, **95**, 350.
217. K. Peeters, P. Grobet and E. F. Vansant, *J. Mater. Chem.*, 1996, **6**, 239.
218. R. Hoppe, G. Alberti, U. Contantino, C. Dionigi, G. S. Ekloff and R. Vivani, *Langmuir*, 1997, **13**, 7252.

219. S. L. Suib, *Chem. Rev.*, 1993, **93**, 803.
220. G. Cao, H.-G. Hong and T. Mallouk, *Acc. Chem. Res.*, 1992, **25**, 420.
221. A. M. Lazarin and C. Airoidi, *J. Inclusion Phen. Macrocyclic Chem.*, 2005, **51**, 33.
222. C. B. A. Lima and C. Airoidi, *Solid State Sci.*, 2002, **4**, 1321.
223. B. Zhang, D. M. Poojary, A. Clearfield and G. Peng, *Chem. Mater.*, 1996, **8**, 1333.
224. P. Gendraud, M. E. de Roy and J. P. Besse, *Inorg. Chem.*, 1996, **35**, 6108.
225. T. Kijima, S. Watanabe and M. Machida, *Inorg. Chem.*, 1994, **33**, 2586.
226. A. M. Lazarin and C. Airoidi, *J. Chem. Thermodyn.*, 2005, **37**, 243.
227. T. Kijima, K. Ohe, F. Sasaki, M. Yada and M. Machida, *Bull. Chem. Soc. Jpn.*, 1998, **71**, 141.
228. V. S. O. Ruiz and C. Airoidi, *Thermochim. Acta*, 2004, **420**, 73.
229. Y. Zhang, K. J. Scott and A. Clearfield, *J. Mater. Chem.*, 1995, **5**, 315.
230. C. B. A. Lima and C. Airoidi, *Thermochim. Acta*, 2003, **400**, 51.
231. C. B. A. Lima and C. Airoidi, *Int. J. Inorg. Mater.*, 2001, **3**, 907.
232. G. B. Hix and K. D. M. Harris, *J. Mater. Chem.*, 1998, **8**, 579.
233. F. Fredoueil, D. Massiot, P. Janvier, F. Gingl, M. B. Doeuff, M. Evain, A. Clearfield and B. Bujoli, *Inorg. Chem.*, 1999, **38**, 1831.
234. C. Airoidi and L. N. H. Arakaki, *J. Colloid Interf. Sci.*, 2002, **249**, 1.
235. R. F. de Farias and C. Airoidi, *Thermochim. Acta*, 2001, **378**, 113.
236. V. S. O. Ruiz, S. L. P. Dias, Y. Gushikem, R. E. Bruns and C. Airoidi, *J. Solid State Chem.*, 2004, **177**, 675.
237. D. M. Poojary and A. Clearfield, *J. Am. Chem. Soc.*, 1995, **117**, 11278.
238. G. Cao, V. M. Lynch and L. N. Yacullot, *Chem. Mater.*, 1993, **5**, 1000.
239. Z.-M. Sun, J.-G. Mao, B.-P. Yang and S.-M. Ying, *Solid State Sci.*, 2004, **6**, 295.
240. K. P. Rao and K. Vidyasagar, *Eur. J. Inorg. Chem.*, 2006, 813.
241. R. M. P. Colodrero, A. Cabeza, P. Olivera-Pastor, A. Infantes-Molina, E. Barouda, K. D. Demadis and M. A. G. Aranda, *Chem. Eur. J.*, 2009, **15**, 6612.
242. C. J. Doonan, D. J. Tranchemontagne, T. G. Glover, J. R. Hunt and O. M. Yaghi, *Nature Chem.*, 2010, **2**, 235.